ADVANCED SUSTAINABLE SYSTEMS
www.advsustainsys.com

Exfoliated Transition Metal Dichalcogenide-Based Electrocatalysts for Oxygen Evolution Reaction

*Michail P. Minadakis and Nikos Tagmatarchis**

The oxygen evolution reaction (OER) has proved to be a hard-to-overlook impediment for the development of water splitting devices, metal-air batteries, or photo-electrochemical cells, to name but a few. Electro- and photo-electrocatalysts, designed using inexpensive materials, that demand low overpotential values to smoothly drive OER in either electrolyzer devices or proton-exchange membrane cells, as well as withstand harsh conditions and repetitive cycling, are fervently desired by the industry. Transition metal dichalcogenides (TMDs), namely MoS_2, WS_2, $MoSe_2$ and WSe_2 as the main representatives, especially when engineered via exfoliation methods, have been highlighted as modular scaffolds for electrocatalytic applications, owed to their ability to have their intrinsic characteristics fine-tuned. In this review, the goal is to highlight the role of exfoliation, as a means of ability engineering, by presenting significant works where these TMDs constitute the core part for OER-catalyzing nanohybrid systems.

1. Introduction

Moving away from the necessity to depend on fossil fuels for our energy needs, the change to alternative energy sources is inevitable. Energy derived from fossil fuels will probably occupy 60% of the total energy needs in 2040, less than 85% of today. Yet, this pattern will have to change to a "non-based on fossil fuels" one, since, according to Millennium Alliance for Humanity and the Biosphere, world's oil reserves will run out by 2052, natural gas by 2060 and coal by 2090. Hydrogen gas (H_2), especially when generated from renewable sources, is considered future fuel for storage and transportation, mostly due to its high energy density (≈140 MJ kg^{-1}), one exceeding that of current fuels, such as coal (24 MJ Kg^{-1}) and petrol (44 MJ Kg^{-1}).[1,2] Currently, 96% of total hydrogen production is based on steam methane reforming (SMR) of mainly fossil fuel-based resources, thus leaving a mere 4% produced by saltwater/water electrolysis. The latter is conducted inside membrane cells called water electrolyzers, which are mainly divided to alkaline water electrolyzers (AWEs), proton- and anion-exchange membrane water electrolyzers (PEMWEs/AEMWEs) and solid oxide electrolyzers (SOEs), that produce H_2 as their main product and chloralkali cells, where H_2 is obtained as byproduct of brine solution electrolysis (**Figure 1**).[2–4] The operating principles of such devices demand substrates that can efficiently catalyze water splitting constituent electrochemical reactions, namely the hydrogen evolution reaction and the oxygen evolution reaction (HER and OER, respectively). In an electrolyzer device, water molecules, in the case of AWEs, are converted to H_2 gas and OH^-, which is eventually oxidized to molecular oxygen or, in the case of PEMWEs, release O_2 gas and free protons, which upon receiving electrons at the cathode, are consumed to drive H_2 production.

The standard Gibbs free energy for water dissociation is estimated to be 237.2 kJ mol^{-1}, corresponding to a voltage of 1.23 V.[6–8] Practically though, the required voltage for a water electrolyzer operation is greater than 1.23 V (mostly even greater than 1.4 V_{cell}), due to extra energy demands needed to overcome thermodynamic and kinetic barriers of the system. The latter mainly stem from OER, which remains the main impediment for water splitting process, since it involves by nature a 4-electron transfer with all intermediate stages being thermodynamically uphill, facts that entail markedly sluggish kinetics and a considerable required anodic potential (overpotential, η), rendering it a both kinetically and thermodynamically unfavorable process.[9] The reaction can occur in both acidic and alkaline environments, with the pH-dependent mechanistic steps being substantially differentiated, yet leading to the same outcome.[9–11] The complete half-reaction is depicted in the following Equations (1) and (2), both in acidic and alkaline conditions (U_0 is the minimum potential needed to drive the reaction:

$$2H_2O_{(l)} \rightarrow O_2 + 4H^+ + 4e^-,\ U_0 = 1.23\ V\ vs\ SHE \quad (1)$$

$$4OH^- \rightarrow O_2 + 2H_2O_{(l)} + 4e^-, U_0 = 0.402\ V\ vs\ SHE \quad (2)$$

M. P. Minadakis, N. Tagmatarchis
Theoretical and Physical Chemistry Institute
National Hellenic Research Foundation
48 Vassileos Constantinou Avenue, Athens 11635, Greece
E-mail: tagmatar@eie.gr

The ORCID identification number(s) for the author(s) of this article can be found under https://doi.org/10.1002/adsu.202300193

DOI: 10.1002/adsu.202300193

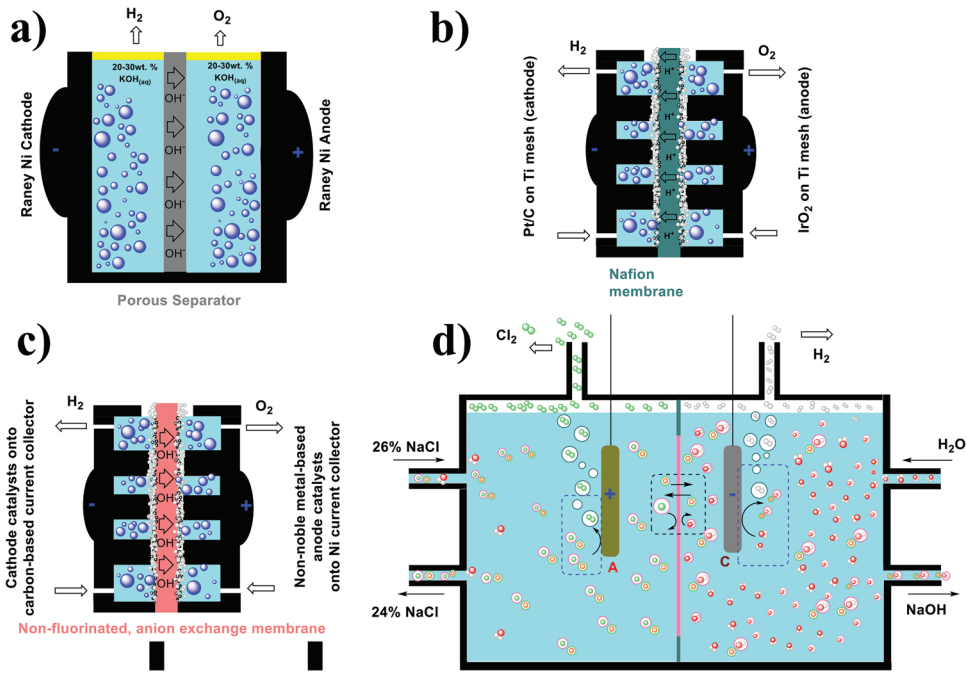

Figure 1. Typical representations of a) AWE, b) PEMWE, c) AEMWE and d) batch chloralkali cell. Adapted with permission.[5] Copyright 2022, American Chemical Society.

Until now, two mechanisms have been proposed to explain the OER process, namely the conventional and most well-studied adsorbate evolution mechanism (AEM) and the newer yet more promising one, lattice oxygen mechanism (LOM).[12] In AEM, a concerted 4-step electron/proton-electron transfer, in alkaline and acidic conditions, respectively, and the formation of OH*, O* and OOH* species (* stands for adsorbed species) in a single, metal-centered, active site, drive the evolution of O_2 molecules.[12,13] In LOM, oxygen vacancies as well as lattice oxygen moieties are taken advantage of, leading to O_2 molecules being partially formed by O originating from both the electrolyte and the catalyst surface, with the reaction taking place in neighboring metal sites.[12,13] The differentiation factor between the two mechanisms lies in the O—O bond formation step. AEM being a metal-redox process, strongly depends on the free energy of the intermediate formation steps, leading to theoretical thermodynamic limitations (it cannot justify electrocatalysts that present overpotentials <370 mV versus RHE).[12] These limitations are nullified with LOM as, in the rate determining step of O-O formation, the bond is directly formed onto oxygen moieties, bypassing the intrinsic characteristics of the metal center.

Taking all the above into account, it is safe to state that designing new classes of OER electrocatalysts is clearly a fervent field of research. In this review, light will be shed on systems that are able to catalyze OER and are based on the, flourishing over the past decades, family of transition metal dichalcogenides (TMDs). More specifically, the aim of this review is to summarize the advances and developments in the field of layered TMDs, engineered through chemically induced liquid phase exfoliation (LPE) and either interfacing OER active compounds or being part of OER catalyzing nanohybrid systems.

2. Overview

2.1. "Status quo" in Energy Production Pathways

As it has been reported, in the long run, fossil fuel-based power generation without the use of any carbon capture and storage technology will have to be entirely discontinued by the end of 21st century. The current situation, which gradually deteriorates, has created a strong incentive to put emphasis on the "hunt" for renewable energy sources, such as wind and solar power.[14,15] Potential future fuel, hydrogen gas, is highly utilized in the chemical industry, where global production is currently estimated to be 500 billion cubic meters per annum.[16] Until now, SMR of fossil fuels make up for 96% of total H_2 production (≈48% from natural gas, 30% from heavy oils and 18% from coal) while electrolyzer devices are responsible for the remaining 4%. Water is unanimously the most interesting source of sustainable hydrogen production and water splitting is considered the "flagship" among the ways of future H_2 production, as SMR of fossil fuels must be slowly abandoned, while its equivalent utilizing biomass as the feedstock is currently at an inadequate technology readiness level (TRL). More importantly, water electrolysis apart from being an almost-zero carbon footprint method, it also produces H_2 gas of higher purity (>99.999%) in comparison to that produced by fossil fuels (≈95%–98%), generates non-toxic byproducts and is easy to be integrated with renewable resources for energy supply.[5] Hydrogen gas purity is pivotal, especially when speaking about fuel cells, where impurities are considered an impediment, eventually leading to lowering of the maximum power output.[17] Consequently, clean energy conversion pathways, such as water dissociation, where electric energy generated from any kind of

power source is converted into hydrogen fuel, reversible fuel cells (RFCs), where hydrogen fuel is produced via electrochemical process, as well as hydrogen storage technologies such as fuel cells, where H_2 is finally utilized and only water is yielded as byproduct and rechargeable and cost/energy-effective Zn-air batteries, which possess exceptionally high energy density are of utmost importance to achieve a sustainable energy landscape.[18–22]

The past decades, hydrogen gas industry has incorporated water electrolysis procedures into the main hydrogen gas production lines and thus, foundations for future dependency on "green" hydrogen, that produced from water splitting, have become more robust. Currently, AWEs are the main kind of electrolyzer device operated in an industrial level, while intensive research on proton-exchange membrane systems and solid electrolytes is being conducted for PEMWEs as well as the technologically immature SOEs to eventually take the lead.[23] AWEs are the typical alkaline electrolyzers, where ≈30%–40% wt. aqueous KOH solution is used as the electrolyte and mostly Ni-based substrates (e.g., Raney Ni) are used as the active electrode coatings. Although, AWEs are by far the most mature and cost-effective electrolyzer device, they suffer from significant issues, such as extensive leakage, due to the liquid nature of the electrolyte, high ohmic drops, which lead to lower current densities entering the system and consequently higher power input to operate, as well as a highly corrosive and oxidative environment that calls for remarkably durable electrocatalysts.[5] In fact, for a water electrolyzer to be viable in industry level, it is imperative that the adorning constituent materials allow it to reach current densities above 500 mA cm^{-2} with applied overpotential below 300 mV and provide durability and robustness.[24] PEMWEs utilizing polymer-based membranes, have undoubtedly resolved the leakage and ohmic drop issues and they have also added to the device development due to their ability to be constructed as small compact devices as well as being able to supply pressurized H_2, eliminating the necessity for extra compression steps.[5] Although PEMWEs may seem as the most suitable alternative due to their higher efficiency as well as compatibility with renewable energy sources, it must be pointed out that, to this day, only noble metal-based substrates are able to operate efficiently under this harsh acidic environment, hence the delay of practically incorporating such devices in the industrial level. Finally, SOEs, which are still researched in small scale level, aim to almost eliminate leakage completely and ohmic drop issues by using solid electrolytes while, having their operating temperatures exceed 900 °C, they need lower electrical energy input to operate.[5] All the above can be pushed one more step forward, by using photoabsorbing substrates, (e.g., TiO_2, CdS or dyes such as porphyrins or phthalocyanines) operating as photocatalysts, thereby leveraging photoelectrochemical (PEC) water splitting and establishing an even "greener" procedure.[25]

Noble metal-based catalysts have been hitherto employed as the benchmark, when comparing the strength of water splitting electrocatalysts, with the striking examples of Pt in carbon matrix (Pt/C) as the HER catalyst at the cell cathode and mostly RuO_2 or even rarer IrO_2 for OER catalysis at the cell anode. Especially in the case of PEMWEs, only PGM (platinum group metals)-based electrocatalysts can withstand the severely acidic environment. More specifically, RuO_2 is commonly employed as the acidic OER electrocatalyst as it has higher abundancy in nature and activity compared to its IrO_2 counterpart.[26] However, it exhibits serious dissolution issues, as it is converted to unreactive RuO_4 salts after long operation times, thus presenting lower long-term stability.[27] Even though IrO_2 is more operationally stable, it has a worse trade-off between efficiency and cost effectiveness, as the pure metal price (500$ per Ir ounce) is a magnitude higher than its counterpart (42$ per Ru ounce), limiting its large-scale use in commercial WS.[28] Although a multitude of non-noble metal catalysts have been developed that outperform the state-of-the-art water splitting electrocatalysts, the applicability of the latter is hard to replace. Consequently, we have reached a state, where the prices of pure noble metals, such as Pt and Ir, have soared in the last decades all due to their slowly depleting natural reserves combined with their increased demand.[29]

2.2. Current Trends in OER Catalyzing Systems

Current issues of designing potent OER electrocatalysts are the observed hurdles of finding materials that can withstand long hours (> 100,000 h) of operation under high voltages (1.8–2.2 V is the current range of operating cell voltages for a commercial PEM cell) and in markedly harsh environments (strongly acidic or alkaline), with an output of at least 1 A cm^{-2}.[30] In order to realize competitive electrocatalysts, certain aspects of their characteristics should be emphasized. More specifically, such an electrocatalyst should catalyze OER with low required overpotential (η) and attain high current in low values of potential, thus having a low Tafel slope that corresponds to faster kinetics. Additionally, it should present low charge transfer resistance (R_{ct}) in the electrode-electrolyte interface as well as have multiple exposed catalytic sites (high electrochemical surface area, **ECSA**) with a high degree of activity per active site (high turnover frequency, **TOF**).[11] Even the state-of-the-art, noble metal-based, rutile-type metal oxide catalysts (RuO_2, IrO_2) that present low values of overpotential and favored kinetics, suffer from agglomeration and poor durability issues, that lead to activity loss, as well as inherent toxicity and dwindling nature reserves.[31]

In view of all the above, it is crystal clear that hydrogen production industry desires to distance itself from the use of PGMs and turn to more sustainable options. Research teams worldwide have invested in designing non-noble metal-based catalysts that would be characterized by both electrocatalytic strength and long-term stability as well as economical and chemical viability. For such an event to take place, both long-term and short-term goals need to be achieved. In the long run, a generic yet substantial goal to overcome the impediments is to delve into the LOM mechanism so that the elements that constitute such an electrocatalyst can be discovered. This way and with the aid of artificial intelligence systems, through screening and theoretical studies of different kinds of electrocatalysts as well as with fine-tuning the redox electrochemistry and surface properties of nanomaterials, engineering of LOM-based electrocatalysts can be achieved.[32] Regarding the surface properties and according to a recent review, the role of defects was highlighted, aiding in the adsorption or even formation of intermediates of a mechanism, and since it plays significant part in overall efficiency, strategies that introduce defects should be followed.[33] Moreover, it has been proved that neutral or semi-neutral conditions could be to some avail,

as there is a chance to diminish both corrosion and instability issues due to harsh acidic or alkaline environment as well as, in the context of practical applications, eliminate the use of membrane separators, eventually lowering the overall operational cost.[34] Additionally, research needs to be focused on catalytic systems that can reach current densities above 1 A cm^{-2} (high current densities-HCD) as these systems can present potential to be incorporated industrially.[35] At HCD conditions, electron transfer behavior changes, leading to increase of catalytic activity, consequently revealing the true profile of the electrocatalyst.

Regarding the short-term approach, the trend in competitive against the state-of-the-art OER-catalyzing systems is to target low-dimension substrates (quantum dots-0D, nanotubes-1D, nanosheets-2D) as well as hollow heterostructures.[35,36] This kind of electrocatalyst engineering will expose more catalytic sites, therefore increasing the specific area and the overall activity, facilitate charge transfer and create short paths for electron transport as well as encourage synergy effects due to optimized electronic properties. Such ventures have already taken place with the use of Pt, Ru and Ir in the form of nanoparticles that also act as a means of lowering the quantity of noble metal used.[37–41] The know-how acquired from this venture could lay the foundations to efficiently drive the improvement of low dimension, non-noble metal-based systems and smoothly transition to the use of such systems.

When targeting large-scale applications, the most promising candidates are carbon-based substrates and transition metal oxide/hydroxides (TMOs). Carbon-based systems are characterized by high electrical conductivity, yet they present low oxidation stability while, even though TMOs lack the proper environment that facilitates electron flow, they have markedly high resistance to harshly corrosive environments.[42] The most interesting carbon-based substrates are defective carbon and heteroatom-doped carbon where, although the first one presents high reactivity, it poses certain challenges for mass-production lines due to the difficult control of defect induction, an impediment that is bypassed by the latter one, which is most suitable for scale-up. Even though oxidation instability of carbon substrates could be partly alleviated by employing the graphitization technique on a high degree, carbon-based nanomaterials would be to more avail if used as the support rather than the active electrocatalyst, facilitating charge transfer.[42] Therefore, TMOs tend to be more attractive due to their desirable activity and high abundance of transition metals (TMs), which entails low electrocatalyst production cost and environmental friendliness. The most common architectures are spinel oxides, which have a lower production cost, and their structure is more easily controllable, perovskite oxides that are characterized by thermal stability, better ion conductivity and redox behavior, which have also been incorporated in small scale, nearly realistic systems, rutile-type oxides such as the representative RuO_2 and IrO_2 and some other types (e.g., layered double hydroxides-LDHs).[42,43] More specifically, Ni-Fe (oxy)hydroxides (NiFe LDHs), especially when they are hollow structured, are the most researched as they present the best trade-off between cost, reactivity, and stability (**Figure 2**).[44,45] Although they still cannot reach industry standards, they offer highly promising ground for further investigation. Different approaches have been followed for their synthesis with the use of metal-organic frameworks (MOFs) being one of great merit for future preparation pathways due to MOFs being a modular scaffold, eventually leading to highly OER-active systems.[46–48]

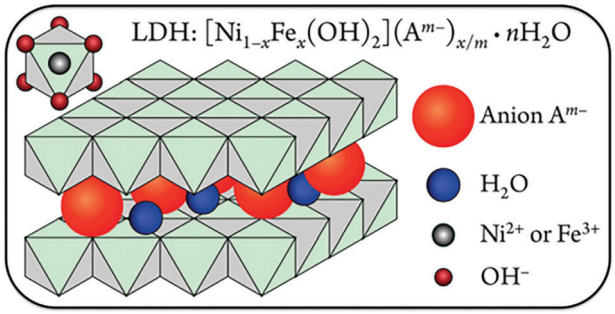

Figure 2. Schematic illustration of the [NiFe]-LDH structure with hydroxyl anions and water molecules being present in the interlayer space. Reproduced with permission.[45] Copyright 2016, Royal Society of Chemistry.

TMOs monopolize the interest in competitive electrocatalyst realization, yet they still face practical issues such as instability in acidic media, poor intrinsic activity, and limited number of active sites.[49] Even though the TMO-based electrocatalyst realization is more mature, there is still room for competitive alternatives. By keeping the element of first-row transition metal, transition metal phosphides, nitrides, dichalcogenides (TMPs, TMNs and TMDs, respectively) have been in the spotlight for the past decades, owed to their higher conductivity due the nature of the metal-P, N and X (X: S, Se, Te) bonds, better corrosion resistance, more exposed active sites, and faster charge transfer.[50] In this review, we will solely focus on the applications of layered TMDs as part of OER catalyzing systems.

3. Transition Metal Dichalcogenides as Electrocatalysts for Water Oxidation

TMDs are considered a promising OER-catalyzing system and have been in the spotlight of electrocatalysis field for the last few years. Notably, TMDs can be divided into two major categories, being the layered (MX_2) and non-layered (M_aX_b) ones, where M is transition metal from groups IVB-VIIB (Hf, Nb, Mo, W, Re) and mostly from group VIIIB (Fe, Co, Ni) for the layered and non-layered ones, respectively, while X is a chalcogen atom (S, Se, Te). In this review, we focus specifically on the applications of layered TMDs of group VIB (Mo, W), since they are the most utilized in the field of electrocatalysis. Briefly, layered TMDs possess a 2D structure analogous to graphene nanosheets, where the motif of a layer comprised of metal atoms "sandwiched" by two chalcogen atom layers, leads to a multilayered system, with a width range 0.6–0.7 nm.[51] Moreover, TMDs exist in three phases with different geometries, being octahedral (1T phase), trigonal prismatic (2H phase), and orthorhombic (3R phase). (**Figure 3**).

The thermodynamic state of group VIB TMDs is 2H phase, in which they present semiconductor characteristics, rendering them attractive to electronic devices applications, while 1T phase is metastable and presents metallic character, being more interesting for electrocatalytic applications.[53] 3R phase is an intermediate non-centrosymmetric phase, which also possesses semiconducting character, yet is more useful in non-linear optical applications.[54]

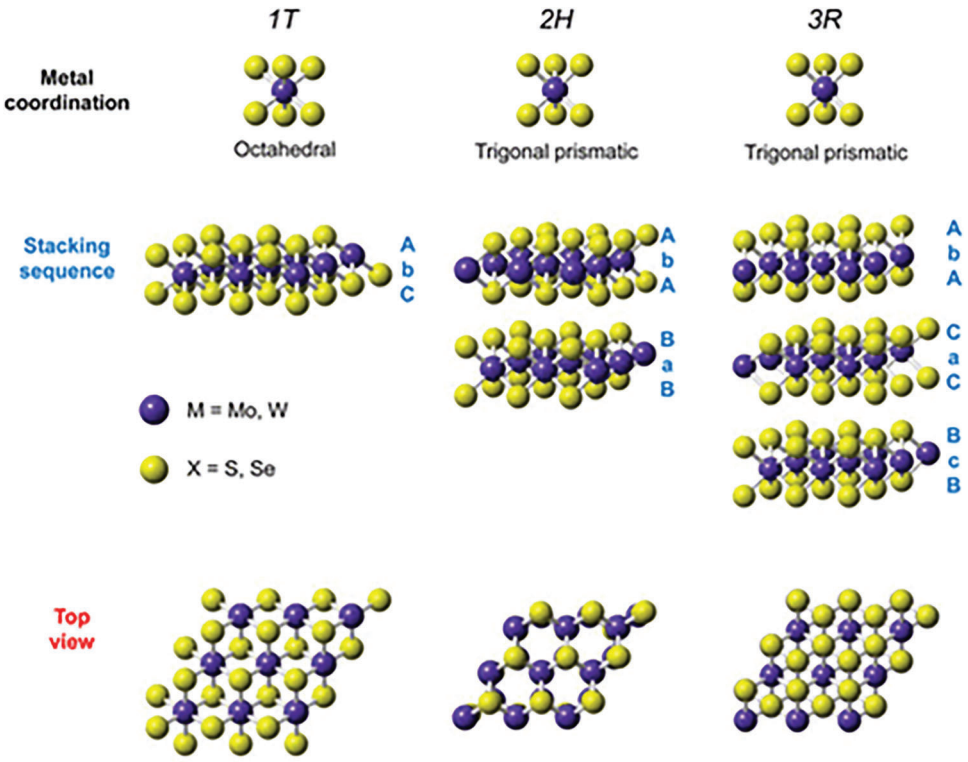

Figure 3. Geometries of different layered TMDs phases (top view and side view). Reproduced with permission.[52] Copyright 2015, American Chemical Society.

With MoS_2 as the main representative, TMDs have drawn attention in the electrocatalysis field, since it has been estimated both theoretically and experimentally, that MoS_2 possesses catalytically active edges, with a free energy of H adsorption almost 0 kJ mol^{-1}, close to benchmark Pt/C catalyst, therefore offering promising ground for HER active catalysts.[55] From its first ever reported work on HER electrocatalysis, MoS_2 and the different metal TMD counterparts, have been considered important contributors in the family of 2D nanomaterials for energy conversion applications. Markedly, they have been the center of review studies, where engineering methods to perfect their electrocatalytic activity are elaborated.[56] Even now, reviews still focus on developments taking place in this field, once again highlighting their importance, and communicating their wide applicability.[57] Layered TMDs also have tunable optical bandgaps, when transitioning from multilayer (indirect bandgap) to monolayer (direct bandgap), with the examples of MoS_2 (1.2 to 1.8 eV) and WS_2 (1.4 to 1.9 eV) being the most characteristic.[58] This allows their incorporation in PEC applications as, additionally, when they are present as either few-layer or monolayer systems, they are characterized by reduced charge recombination.[50]

However, TMDs also present shortcomings, with the most important being the basal plane inactivity of bulk material, which possesses semiconducting character. Consequently, only a few of the many potential active sites are available and conductivity along the surface exhibits anisotropy.[59] Fine-tuning TMDs properties, via defect engineering, phase, and bandgap transition as well as chemical modification, is one of the most critical advantages they possess. The most efficient way to realize these changes is through the process of chemically induced exfoliation, a procedure that "unlocks" their true potential.[51,60]

A plethora of pathways are available to produce low dimensional TMD that can be either bottom-up methods, where inorganic salt precursors are used as the starting point or top-down methods, where bulk 3D material is the scaffold. Bottom-up procedures can be divided into hydrothermal/solvothermal, deposition (chemical, atomic layer, electrochemical and thermal) as well as solid-phase synthesis (**Figure 4**).[61] Bottom-up methods can achieve high quality nanoscale materials with controllable thickness via simple and efficacious procedures, yet they are also characterized by non-controllable uniformity of the final product, harsh conditions in terms of applied temperature and pressure, thus a high operational cost in mass production level. Conversely, chemically induced exfoliation, micromechanical cleavage, ball milling and laser thinning constitute the top-down methods (Figure 4).[61] Micromechanical cleavage can produce mono/few-layered nanosheets of high quality yet it lacks uniformity and is characterized by low yield, incompatible with the industry demands. Ball milling is a low-cost and easily scalable method, yet it produces highly defective material and the need for strict conditions increases the operational cost. Consequently, LPE is the most promising method for industry standards as apart from being cost-effective and large-scale-friendly, its simplicity, characteristics control, high yield, ability to dope the lattice and/or modify the TMD structure, constitute the appropriate profile for utilization in mass production, with its only downside being the lower quality in terms of dimensions final material.[62,63]

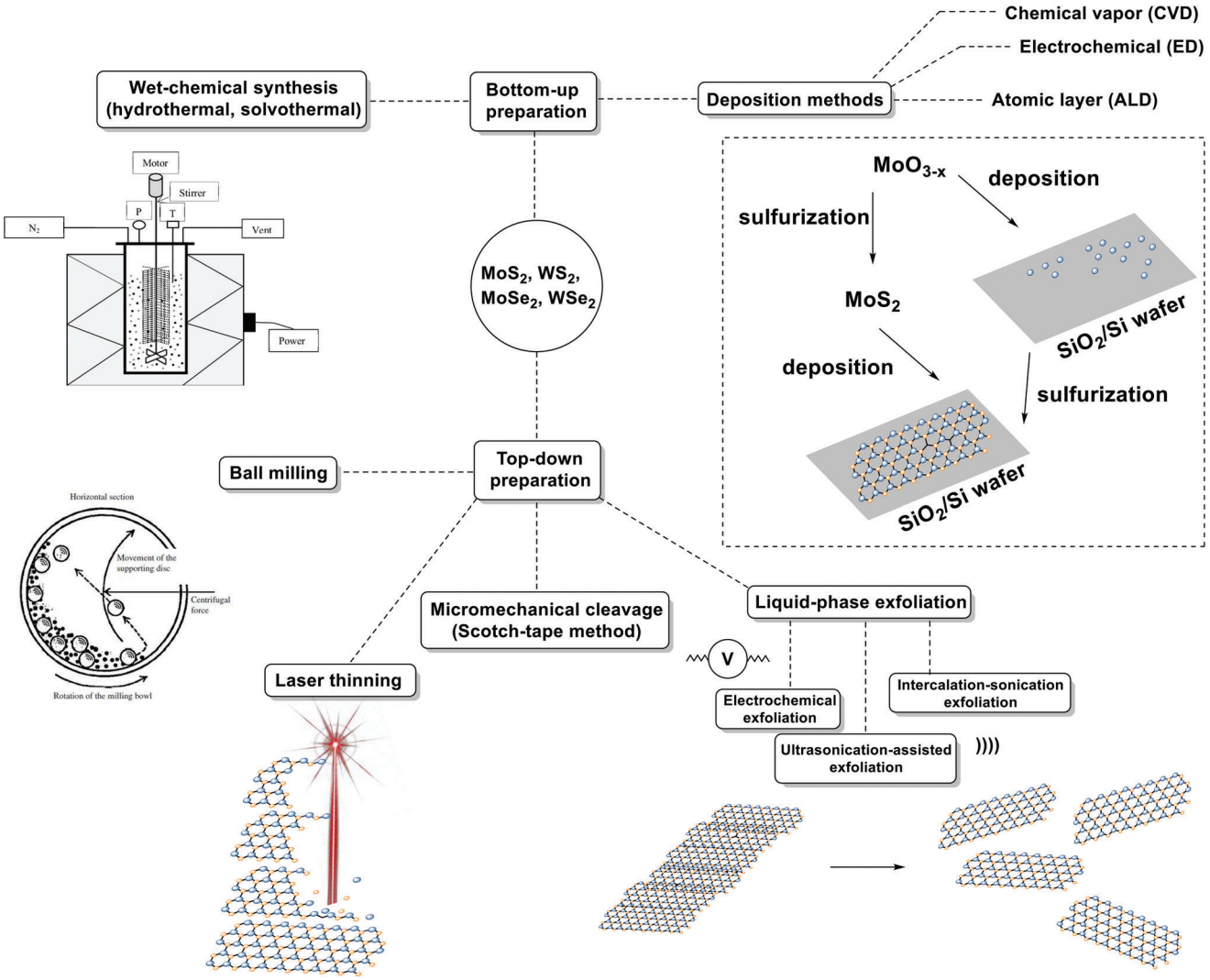

Figure 4. An illustrative synopsis of transition metal sulfides/selenides (TMS) bottom-up and top-down synthetic methodologies.

While LPE, mediated by Li-intercalation, is known from 1980s, the foundations for the research-level accessible wet exfoliation method were recently laid.[64,65] Wet exfoliation approaches, utilizing either solely the properties of solvents or with the complementary use of surfactants and using ultrasonication as the agitation method, either in small or larger scale, of a broad spectrum of bulk materials (graphite, h-BN, TMDs, TMOs, metal halides, LDHs, metal carbides/nitrides etc.) were reported, establishing this technique and adding another "arrow" in the 2D material preparation and engineering "quiver".[60,66,67] The past decade, the field of wet exfoliation pathways has expanded with the introduction of high shear mixing as the agitation method in solvent-based LPE as well as the use of externally applied voltage as the stimulus (electrochemical exfoliation) that drives the process.[68,69] Furthermore, it was only recently that the well-studied, scalable intercalation/exfoliation strategy was applied in a wider range of semiconductor materials (In_2Se_3, InSe, Bi_2Se_3), demonstrating that it is yet to reach the maximum potential of this strategy.[70] Other research groups pushed the boundaries of this field of knowledge by expanding LPE applicability in more solvents and with the aid of strongly acidic environment (e.g., chlorosulfonic acid), thus allowing phase tunability of the TMD scaffold (Li-interacalation LPE leads to 1T-TMD, while chlorosulfonic acid-aided LPE leads to 2H-TMD, **Figure 5**).[71,72] By retaining semiconducting character in the exfoliated material, the basal plane is kept intact, the absence of electrical charges facilitates interaction with electroactive species and the increased number of sulfur vacancies allows chemical modification of the edges via covalently interfacing active substrates through bonding with thiol or disulfide containing organic molecules.[73–75] Conversely, by preparing exfoliated, metallic TMD, bifunctionality of the catalyst can be achieved since 1T-TMDs have high activity in HER. Moreover, the introduction of charges can be utilized either non-covalently, through interfacing moieties via electrostatic interactions, or in a covalent fashion by exploiting the nucleophilic character of S^- and decorating the basal plane.[76–78]

Since a multitude of works involving different pathways to exfoliation arose, it was expected that the field of TMD applications

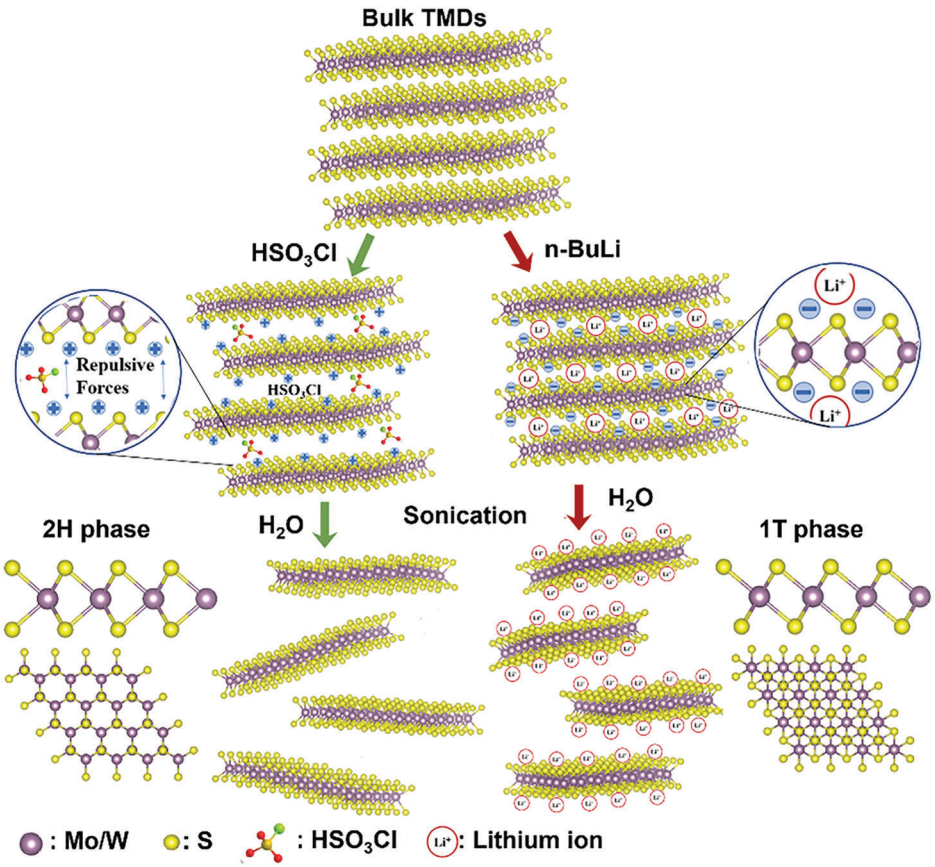

Figure 5. Liquid phase exfoliation routes for bulk 3D TMDs (Left: HSO_3Cl-assisted exfoliation, right: n-BuLi assisted exfoliation). Reproduced with permission.[79] Copyright 2022, American Chemical Society.

would expand. Some recent works that highlight the electrocatalytic activity in HER involve exfoliated MoS_2 deposited on a carbon cloth electrode, exfoliated WS_2 catalytically enhanced by Ag nanoparticles, prepared with the use of supercritical fluid, defect rich $MoSe_2$ and wet exfoliated WSe_2-WO_3 structure, under either acidic or alkaline conditions, and are owed to the S-vacant edges affinity for H atoms.[80–83] As proved by a recent theoretical study of TMD monolayers, S^- as well as Mo-edges are also responsible to bind intermediate products (OH*, OOH*, O*), emerging during OER catalytic cycles.[84] However, the inability to strongly bind these species has impeded the practical use of TMDs in their current form as whole WS electrocatalysts.

OER calls for highly durable electrocatalysts that can withstand long hours of operation in harsh environments (strongly acidic/alkaline and highly oxidative), should they aim to be incorporated into realistic systems. Even though transition metal oxides/hydroxides offer these characteristics, as mentioned above, they also possess low conductivity, and they exhibit dissolution problems and agglomeration issues. TMDs can resolve the electron flow disadvantage of TMOs due to their highly conductive surface, especially when present in their metallic phase. Furthermore, although Mo edges in TMD lattice offer O-related species adsorption spots, the TMD itself does not possess intrinsic activity in OER. In most cases, the OER activity of TMD-based systems originates from the components interfaced with the TMD. As supporting evidence stands, even TMOs formed onto the TMD surface through oxidative pathways, do not enhance OER activity as the M-O (M: Ti, V, Cr, Cu, Mo, Ta, W, Re, Os) bond strength does not have the proper energy to promote the reaction.[85,86] The exfoliation approach as an economically viable and high throughput means, offers high tunability in terms of size and phase engineering. This way, mono-layered systems can be realized, that can be exploited for photo-related applications. Also, TMD phase can be engineered by introducing S-defects that can be chemically modified as stated above, eventually leading to systems where the activity may arise from sole atoms (single atom catalysts-SACs). Furthermore, introduction of charges can also be achieved leading not only to modification scaffolding but also to bifunctional systems as the metallic phase is known to be remarkably active in HER. What is more, interfacing photoactive compounds can allow the incorporation of TMD-based hybrids in PEC cells that can further extend this capability to solar-operating devices.

Even though works elaborating different combinations of TMDs with HER activity enhancing elements have been sprawling the past decades, only few works studying them as OER electrocatalysts have been reported. In more detail, the TMDs involved in such applications are synthesized via bottom-up pathways. For instance, MoS_2 nanocrystals deposited on Co foam or enclosed in a N-doped carbon framework exhibited of the lowest overpotential values to reach benchmark current density

10 mA cm^{-2} (η_{10}) reported, needing 270 and 390 mV.[87] Mesoporous WS_2 prepared in situ on Ni foam also exhibited η_{10} value <350 mV while hollow $MoSe_2$ nanocubes and WSe_2 nanosheets doped with $CoSe_2$ nanoparticles, also showed low η_{10} values (309 and 330 mV, respectively) as well as favored kinetics (Tafel slope values were 84 and 76 mV dec^{-1}, respectively).[88–90] It was only during the recent 5–10 years that these TMDs, engineered through exfoliation procedures, have started to be utilized in OER electrocatalysis. This review, with focus on OER electroactivity, will comprehensively address the advances in the field of exfoliated layered TMDs interfacing OER active compounds.

Regarding the knowledge available, a comprehensive review of systems based on exfoliated layered TMDs as electrocatalysts for OER is missing. Excellent reviews about TMD-based electrocatalysts in either solely OER or full water splitting exist in literature.[91–93] The aim of this review is to summarize the advances and developments in the field of TMDs engineered through chemically induced, wet phase exfoliation, interfacing OER active elements and leading to hybrid systems that act as electrocatalysts in water oxidation, in alkaline or neutral electrolyte. The practical purpose of the exfoliation approach will be highlighted as it is considered a means that could be incorporated by industry to facilitate the engineering of highly potent water splitting electrocatalysts. Therefore, it is vital to disseminate the work done in this specific field to encourage more research groups to contribute to this venture and to uncover the so far unseen capabilities of TMDs engineered with this strategy.

3.1. MoS_2 as Electrocatalyst for Water Oxidation

While MoS_2 is the most well-known and well-studied among the layered TMDs, only a handful of works have utilized exfoliated MoS_2 as part of an OER electrocatalytic system. The following works will present MoS_2 either demonstrating its intrinsic OER strength, along with some kind of support (e.g., carbon nanotubes, etc.) or interfacing an OER active element (e.g., TM nanoparticles, metal-porphyrins, etc.), thus relying on synergetic phenomena.

The role of 1T-MoS_2 in electrocatalysis of oxygen-related reactions (OER/ORR) has been highlighted through formulating a hybrid 1D-2D structure with oxidized carbon nanotubes (oCNTs) while investigating its performance on lithium-oxygen batteries (LOBs).[94] LOBs are considered as probably the most efficient alternative to the Li-ion batteries (LIBs), as, theoretically, they can feature markedly higher specific energy (3500 W h Kg^{-1}) than LIBs (current limit ≈300 W h Kg^{-1}, at cell conditions). Furthermore, they keep the induced voltage ≈3 V, while most LIB materials achieve barely more than 260 mAh g^{-1} with voltages higher than 4.6 V, thus challenging the stability of the electrolyte.[95] However, such systems are yet to operate since they require a cathode material that can withstand a great number of charge-discharge cycles. oCNTs were used both as a means of preventing restacking of 1T-MoS_2 nanosheets and to promote synergy with the TMD at the interface. The hybrid system was tested in aqueous 0.1 M KOH solution for O_2 evolution, where it exhibited an enhanced performance (see **Table 1**) compared to 1T-MoS_2 alone (290 mV), at the benchmark current density of 10 mA cm^{-2} (η_{10}), while it was found superior to the 2H-MoS_2/oCNTs equivalent (440 mV). The metallic character of the TMD allowed the maximization of catalytic sites as both the Mo edges and the TMD basal plane are active, while its high electrical conductivity facilitated the charge transfer process onto the TMD and along the TMD/CNT interface. The pivotal role of metallic MoS_2 was also proved by the lowered values of charge-transfer resistance (R_{ct}, 84 *vs.* 357 Ω of the 2H counterpart) as well as double layer capacitance (C_{dl}) where the latter entailed almost tenfold increase in **ECSA** (84.7 *vs.* 9.7 cm^2 of the 2H counterpart). This remarkable performance on OER along with its ORR activity, were translated into a promising cathode material in LOB testing operation. The 1T-MoS_2/o-CNT hybrid exhibited lowered charge and discharge overpotentials by 300 and 200 mV, respectively, at the half of the upper-limit capacity, 250 mA h g^{-1}. In more depth, the system was found to withstand more than 100 charge-discharge cycles at the maximum capacity of 250 mA h g^{-1}, owed to the formation and decomposition of Li_2O_2 at the charge and discharge, respectively, arising from an electrochemical activation phenomenon. 1T-MoS_2 activity is markedly enhanced by the stabilization oCNTs provide and the synergy between materials of different core, fact reflected on the decrease of charge-discharge overpotential at the upper-limit capacity (**Figure 6**).

On a different note, the impact of NiO_x nanoparticles (NPs), a known active OER compound, was assessed when interfaced with 2H-MoS_2.[96] NiO_x nanostructures have proved to be efficient against water oxidation, due to their innate stability and the facilitation of $NiOOH^*$ intermediate formation, which drives the reaction.[97] By mixing solutions of exfoliated 2H-MoS_2 nanoflakes and NiO_x NPs, a nanocomposite with the NPs decorating MoS_2 surface was realized. Considering the noticeable onset value at 1.5 V versus RHE and the quite low Tafel slope (78 mV dec^{-1}) that led to the highest current density recorded (≈60 mA cm^{-2}) at 1.8 V, this system appeared as a promising water oxidation electrocatalyst (see Table 1). Ni centers serving as the active sites, combined with the flow of electrons at MoS_2 surface and the enhanced stability offered by their nestling on the lattice, lead to a cost-effective, yet potent system.

By modulating the interface of Mo_2C onto nickel foam (NF) electrode with MoS_2 QDs, a nanocomposite with high electrocatalytic strength on OER was furnished.[98] Mo_2C nanostructures are desirable substrates for future electrocatalyst realization due to their high conductivity and tendency to exhibit good synergetic effects when interfaced with electroactive species.[99] Formation of a Mo_2C layer onto NF was followed by incorporating via a solvothermal method, chemically exfoliated MoS_2 nanosheets and allowing them to vertically align onto the active surface area, exposing larger contact spots and facilitating charge transfer. The heterostructure exhibited metallic characteristics, owed to metallic character of Mo_2C, therefore accelerating electron mobility. The nanocomposite exhibited an excellent OER performance (see Table 1), marginally better than benchmark RuO_2 (120 mV), yet far superior from any of all the reference materials. Lower R_{ct} (1.704 Ω) than its component materials alone (1.827 and 1.846 Ω, for MoS_2 and Mo_2C on NF, respectively) and a Tafel slope directly comparable with the one of RuO_2, confirmed the enhanced conductivity and encouraged electron transport. This is attributed to synergistic effects taking place at the interface of the two materials. The electron accumulation at the interlayer space led, due to inherently high conductivity of NF, to electrons moving from Mo

Table 1. Synopsis of water oxidation electrocatalysts reported in works outlined in this review.

Active Substrate	Supporting electrolyte and activity	Durability	Double-layer capacitance [C_{dl}] [mF cm^{-2}]	η_{10} [mV]	Mass loading [mg cm^{-2}]	Tafel slope [mV dec^{-1}]	R_{ct} [Ω]	Reference
1T-MoS_2/oCNTs	O_2 sat. 0.1 M KOH, **Li-O_2 batteries, OER**/ORR	No change in charge-discharge voltage over 100 cycles at max. capacity of 500 mAh g^{-1}	27	270 vs RHE, **GCE**	≈0.32	N/R	83.6	[94]
1T-MoS_2/NiFe-LDH	N_2 sat. 1 M KOH, **OER**/HER	≈0% overpotential drop after 10 h	N/R	210 vs RHE, **GCE**	≈0.21	46	48	[103]
2H-MoS_2/NiO_x NPs	N_2 sat. 1 M KOH, **OER**/HER	N/R	N/R	≈370 vs RHE, **GCE**	N/R	78	N/R	[96]
2H-MoS_2/BPQD	N_2 sat. 0.1 M KOH, **OER**/HER	≈0% current loss after 15 h	N/R	370 vs RHE, **GCE**	≈0.24	46	46	[104]
2H-MoS_2 QDs@Mo_2C@NF	N_2 sat. 1 M KOH, **OER**	0.05% current loss after 100 h	15.5	110 mV vs RHE, **NF**	≈2.35	57	1.7	[98]
2H-MoS_2/CoP nanoparticles/N, P co-doped carbon framework	O_2 sat. 1 M KOH, **Zn-air batteries, OER**/ORR/HER	≈0% current loss after 24 h	1.86 mF	306 vs RHE, **GCE**	≈0.56	67	7.7 Ω cm^2	[100]
2H-MoS_2/LSCO nanoparticles-GNS	N_2 sat. 1 M KOH, **OER**/HER	≈18% current loss after 12 h	N/R	436 vs RHE, **CC**	N/R	69.6	25	[105]
Electrostatically bound 2H-MoS_2/MWCNTs heterostructure	O_2 sat. 0.1 M KOH, **OER**/ORR	N/R	N/R	550 vs RHE, **GCE**	N/R	82	N/R	[102]
Ni decorated 1T-WS_2	N_2 sat. 0.1 M KOH, **OER**	N/R	N/R	350 vs RHE, **GCE**	≈0.07	51	N/R	[112]
2H-WS_2@Ni_2O_3 nanorods (WS_2-r)	Ar sat. 1 M KOH, **OER**	≈3% overpotential drop after 10 h (10 mA cm^{-2})	1.76	334 mV	N/R	67.7	2.21	[113]
2H-WS_2 bearing Ni porphyrin	N_2 sat. 0.1 M KOH, **OER**	≈0% overpotential increase after 10000 cycles	0.05	600 mV vs RHE, **GCE**	≈0.16	83	47	[114]
2H-$MoSe_2$/CdS nanohybrid dots	O_2 sat. 0.1 M KOH, **OER**/ORR	≈12% current loss after 36 h	N/R	460 mV vs RHE, **PGE**	≈1.22	66	360	[118]
2H-$MoSe_2$/Mo_2C/SWCNTs	N_2 sat. 0.5 M H_2SO_4 and 1 M KOH, **OER**/HER	≈81% and ≈64% current loss after 30 min. in acidic and alkaline conditions, respectively	N/R	197 mV(H^+)/241 mV (OH^-) vs RHE, **GCE**	≈2.08	N/R	N/R	[116]
Co/Ni nanoparticle decorated 2H-$MoSe_2$	Ar sat. 1 M KOH, **OER**/HER	≈0% current loss after 10 h (10 mA cm^{-2})	0.0025	378 mV vs RHE, **GF**	0.3	170	4	[117]
2H-WSe_2/CdS nanohybrid dots	O_2 sat. 0.1 M KOH, **OER**/ORR	≈12% current loss after 36 h	N/R	290 mV vs RHE, **PGE**	≈1.22	49	260	[118]
2H-WSe_2/N, S-doped rGO/NiFe-LDH	N_2 sat. 1 M KOH, **OER**/HER	≈0% overpotential increase after 50 h (50 mA cm^{-2})	N/R	260 mV vs RHE, **NF**	≈1	86	0.6	[120]

[a] All measurements reported in this review were conducted at 25±5 °C; [b] **RHE**: reversible hydrogen electrode, **GCE**: glassy carbon electrode, **NF**: nickel foam, **CC**: carbon paper, **PGE**: pencil graphite electrode, **GF**: graphite foil; [c] N/R stands for not reported.

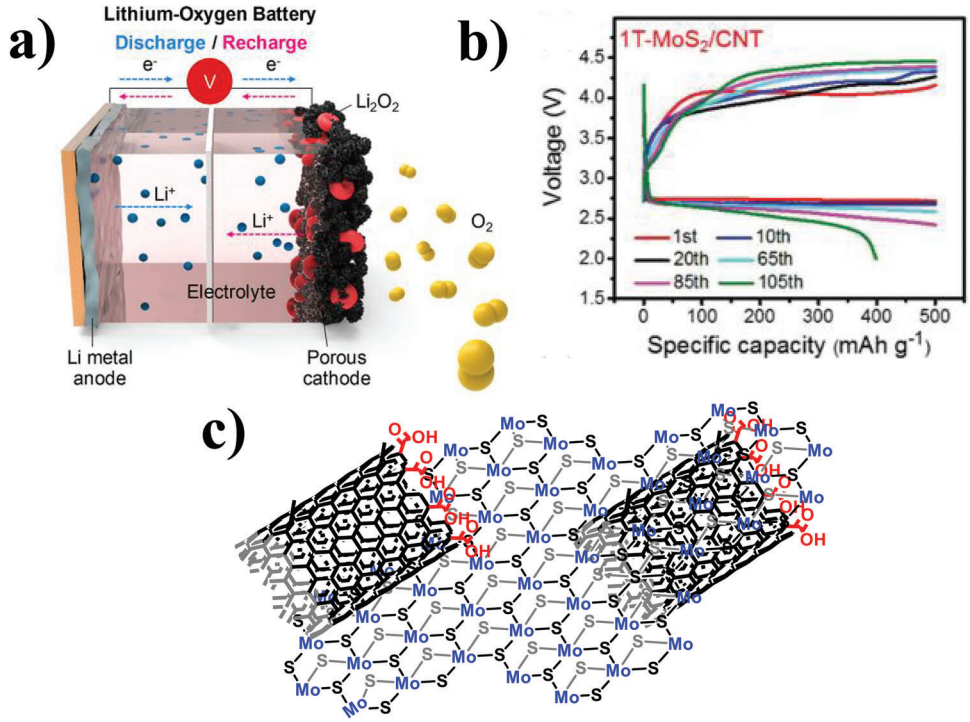

Figure 6. a) Schematic representation of a Li-O_2 battery. Reproduced with permission.[95] Copyright 2020, American Chemical Society, b) Discharge/charge curves of LOBs with the 1T-MoS_2/CNT cathode at a current density of 200 mA g^{-1} with an upper-limit capacity of 500 mA h g^{-1} for over 100 cycles. Reproduced with permission.[94] Copyright 2018, Royal Society of Chemistry. c) Schematic representation of 1T-MoS_2/o-CNT nanohybrid.

centers of Mo_2C to S centers of MoS_2. Gathering of electrons at S sites, which acted as the adsorption sites for OH^* intermediates, increases the affinity for the adsorbents.

There has also been works where an electrocatalytically active MoS_2-based ensemble could benefit from a robust and full of defective carbon matrix. Such an example is a trifunctional electrocatalyst for overall WS and Zn-air batteries operation, based on exfoliated MoS_2 nanosheets embedded on N, P-co-doped carbon framework (NPC) and decorated with cobalt phosphide (CoP) nanoparticles.[100] In this nanohybrid, NPC was the substrate to host the catalytically active elements as well as to enhance catalytic activity due to its great amount of pyridinic-type N atoms and defects, acting as adsorption sites. CoP, known to possess catalytic strength for OER/ORR/HER, was used both as electrochemically active element as well as a means of preventing MoS_2 aggregation.[101] In an aqueous 1 M KOH solution, the system exhibited an η_{10} value of 306 mV (see Table 1), lower than RuO_2 (315 mV) and CoP/NPC (319 mV) as well as the lowest Tafel slope (67 mV dec^{-1}) and highest **ECSA** (46.5 cm^2) among precursor materials, owed to synergy between different elements. In more detail, the defective pyridinic-type N spots offer bridging points for the heterostructure of MoS_2 nanosheets and CoP particles to form. When such a connection is established, the interface between the components allows faster charge transfer and more active adsorption sites, thus giving rise to multiple electrocatalytic activity. Negligible changes were observed in recorded current at chronoamperometry for 24 h, also demonstrating remarkable stability for the nanohybrid. Considering its overall superiority, this system was also tested in near-realistic applications such as a complete electrochemical cell and a Zn-air battery setup. In more detail, it exhibited a really close to benchmark voltage (1.67 *vs.* 1.61 V of 20% Pt/C-RuO_2 pair) with a constant *I-t* curve over the course of 24 h for overall water splitting, while also presenting a higher maximum capacity of ≈776 mAh g^{-1} compared to 705 mAh g^{-1} of 20% Pt/C-RuO_2 pair.

A nanocomposite consisting of multi-walled carbon nanotubes (MWCNTs) and exfoliated MoS_2 was formulated and screened as bifunctional catalyst for ORR and OER (**Figure 7**).[102] Positive charges on MWCNTs were introduced via a surfactant-assisted debundling procedure, while negative charges on MoS_2 were introduced via an equivalent surfactant driven LPE. The nanohybrids were realized by mixing both components in a 3:1 ratio TMD:MWCNTs in aqueous medium, where, via electrostatic interactions, the species came into contact. It is noteworthy that when observing scanning electron microscopy (SEM) micrographs of the MoS_2 bearing system, MoS_2 nanosheets and debundled MWCNTs alternate, with the latter detected at the TMD basal plane, leaving the edges exposed. Electrocatalytically, in an O_2-saturated 0.1 M KOH solution, MoS_2-MWCNTs showed a more promising picture of an effective OER electrocatalyst with an almost 18 mA cm^{-2} current density recorded at an overpotential of 550 mV (see Table 1). Tafel slopes further supported the noteworthy nanohybrid performance with MoS_2-MWCNTs presenting a value of 82 mV dec^{-1}, almost equal to the state-of-the-art (i.e., RuO_2 with 86 mV dec^{-1}).

There have also been some works where, even though exfoliated MoS_2 is not the core element in OER electroactivity, it adds to the system of bifunctional and trifunctional hybrids or is even

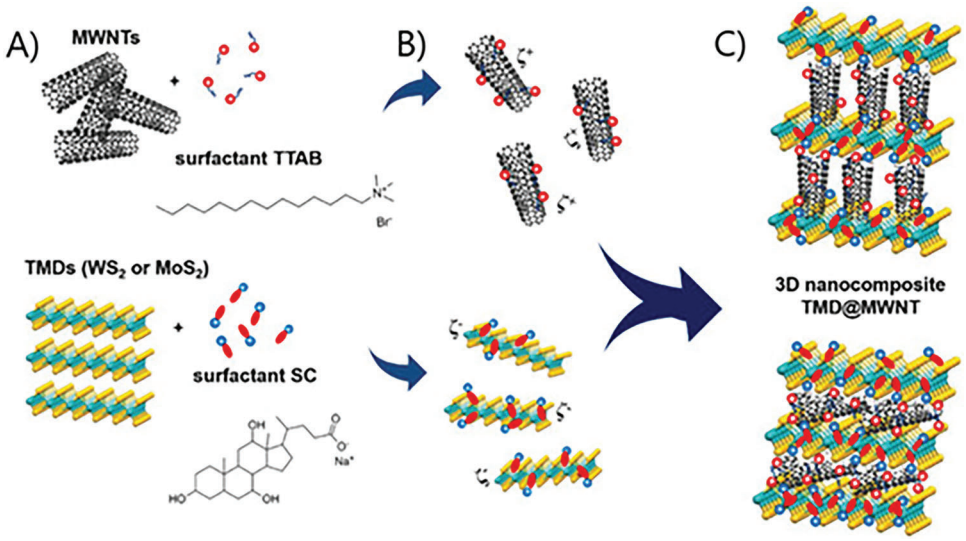

Figure 7. Schematic illustration of the electrostatically bound 3D TMD/MWCNTs nanocomposite. Reproduced under the term of CC-BY license.[102] Copyright 2021, The Authors, published by MDPI.

incorporated in nearly realistic applications. Specifically, 1T-MoS_2 has been part of a superlattice structure, interfacing the highly promising NiFe-LDH for overall WS.[103] Based on the fact that heterostructures of 1T-MoS_2/graphene and NiFe-LDH/graphene are active in HER and OER, respectively, as proved in this work, a potential bifunctional catalyst was targeted, by combining the active element of each hybrid. Negatively charged MoS_2, produced by Li-intercalation mediated LPE and positively charged NiFe-LDH, produced by ion exchange-exfoliation, were brought together to form an electrostatically bound superlattice structure. In aqueous 1 M KOH solution, the latter exhibited remarkable activity in HER and markedly low η_{10} for OER (see Table 1), directly comparable with that of benchmark RuO_2. The nanohybrid was also tested in a water splitting cell, applied as both the cathode and the anode and η_{10} was found 340 mV while only 140 additional mV were needed for 50 mA cm^{-2}, demonstrating a promising profile for an AWE application. Another rationally designed system between black phosphorus (BP) that possesses OER activity and MoS_2 that exhibits affinity for HER intermediates was also realized, targeting again a potential bifunctional nanohybrid.[104] A 5:1 mixture of bulk MoS_2 and BP was electrochemically exfoliated and an electrostatically bound 0D/2D heterostructure was furnished (MoS_2-black phosphorus quantum dots/BPQD), presenting bifunctional character in alkaline electrolyte (0.1 M KOH) with a better than bare MoS_2 HER performance and a superior to BP OER activity (see Table 1). In a more recent work, a bifunctional catalyst based on exfoliated MoS_2 decorated with LSCO NPs (nanoparticles containing La, Sr and CoO_x) onto a surface of exfoliated graphene nanosheets (GNS) was realized.[105] Perovskite oxide LSCO NPs, as a cost-effective, OER active component, decorated MoS_2 surface and finally a chemical welding step gave rise to the whole electrode (hybrid-CW). Hybrid-CW presented slightly worse performance than its precursors (see Table 1), yet it was compensated for its bifunctional character. Consequently, it was tested in a complete cell where η_{10} was found to be 520 mV, while its performance remained stable over the course of 12 h, except for a ≈18% decrease in anodic current. Overall, this system's performance could be deemed applicable for AWE systems and the fact that inexpensive materials and techniques were utilized highlights this potential even further.

3.2. WS_2 as Electrocatalyst for Water Oxidation

Surprisingly, less attention has been paid at WS_2 in the field of electrocatalysis compared to MoS_2, yet it possesses some superior characteristics, such as better conductivity and an even higher direct bandgap when being few layered, justifying its suitability for PEC applications.[106] This is confirmed by the number of works that involve WS_2 in PEC applications, which will be discussed next. Mainly, metal oxides have been considered suitable as water splitting photo-electrocatalysts, yet their weak absorption in the visible region as well as their more positive than the thermodynamic potential of water oxidation valence band maximum, which leads to redundant, thermally lost energy, hold them back in the field of photovoltaics.

A type II heterojunction, consisting of WS_2 and MoS_2 nanosheets, produced via LPE, with an aim to test the potential of this synergy in a solar-powered, complete WS cell was investigated.[107] Specifically, in acidic conditions with aqueous $HClO_4$ as electrolyte, such a heterojunction demonstrated a lower cell onset overpotential and an increased photocurrent (Hg lamp, 1.4 W cm^{-2}), by one and two orders of magnitude, respectively, compared to individual WS_2 and MoS_2, owed to the enhanced absorption in the Vis region (see **Table 2**). Finally, the heterojunction incident photon to current conversion efficiency (IPCE) value was found greater than that of the constituent materials.

Another type II heterojunction of a mixture of exfoliated WS_2 and MoS_2 nanosheets was realized onto hydrothermally grown on highly porous W, WO_3 nanoflakes for the PEC water splitting.[108] In more detail, 2D 2H-WS_2 and 2H-MoS_2

Table 2. Synopsis of photo-electrocatalysts for water oxidation reported in works outlined in this review.

Active Substrate	Supporting electrolyte and activity	Durability	Maximum current [mA]	Maximum photocurrent [mA cm^{-2}]	Faradaic efficiency [%]	IPCE	ABPE	R_{ct} [Ω]	Reference
2H-MoS_2/2H-WS_2 heterojunction	Ar sat. 0.5 M $HClO_4$, Photoelectrochemical **water oxidation**	≈25% current loss after chronoamperometry for 200 s	N/R	≈0.4 mA cm^{-2} at 1.15 V vs RHE, **FTO-coated glass**	67%	≈0.1% at 600 nm	≈0.1% at 600 nm	N/R	[107]
2H-WS_2/MoS_2/W-WO_3 heterojunction	0.5 M H_2SO_4, Photoelectrochemical **OER in water splitting**	≈0% current loss after 10000 s	≈15 mA cm^{-2} at 1.23 V vs RHE	≈1.7 mA cm^{-2}	N/R	N/R	N/R	19.25 Ω cm^{-2}	[108]
2H-WS_2/WO_3 heterojunction	0.5 M Na_2SO_4, Photoelectrochemical **OER in water splitting**	N/R	N/R	≈6.6 mA cm^{-2} at 1.75 vs SCE, **thin film**	N/R	≈55% at 350 nm	≈2.3% at 0.75 V vs SCE	N/R	[109]
α-Fe_2O_3/2H-WS_2/WO_x nanostructure	1 M NaOH, Photoelectrochemical **water splitting**	≈0% current loss after 24 h	≈2.1 mA cm^{-2} at 1.23 V vs RHE	≈0.98 mA cm^{-2} at 1.23 V vs RHE, **thin film**	≈84%	≈15.5% at 325 nm	N/R	423.1 Ω	[110]
1T-WS_2/TiO_2 nanoarrays	0.5 M Na_2SO_4, Photoelectrochemical **water oxidation**	≈9% photocurrent loss after 5 h	≈1.8 mA cm^{-2} at 1.8 V vs RHE	≈0.88 mA cm^{-2} at 1.4 V vs RHE	N/R	N/R	N/R	108.1 Ω	[111]

[a] All measurements reported in this review were conducted at 25±5 °C; [b] **RHE**: reversible hydrogen electrode, **GCE**: glassy carbon electrode, **NF**: nickel foam, **CC**: carbon paper, **PGE**: pencil graphite electrode, **GF**: graphite foil, **SCE**: standard calomel electrode, **FTO**: fluorine-doped tin oxide, **IPCE**: incident photon-to-current conversion efficiency, **ABPE**: applied bias photo-to-current conversion efficiency; [c] N/R stands for not reported.

Figure 8. Schematic illustration of WS_2-WO_3 heterojunction (100 mW cm^{-2} illumination, 0.5 M Na_2SO_4 as the supporting electrolyte). Reproduced with permission.[109] Copyright 2021, Elsevier.

nanosheets were furnished via LPE and their mixture was electrochemically deposited onto WO_3 surface by applying bias voltage for different time periods. The system performed optimally when the deposition lasted for 240 s, whereas more prolonged timespans, i.e., 360 s, led to stacking of the nanosheets and consequent loss of their activity, due to concealment of active edges. The synergy between WS_2/MoS_2 composite, which was shown to exhibit improved conductivity as well as reduced charge carrier recombination rate and WO_3, that offers a vast surface area along with oxygen desorption paths, are the reasons for the reported potential of the system. With the deposition of one component onto WO_3, a 36% increase in current density was observed. On the contrary, when the TMD-based heterojunction was used instead, an improvement of 340% was recorded, always with respect to WO_3 alone. In aqueous 0.5 M H_2SO_4 electrolyte, the WS_2/MoS_2-WO_3 system reached the impressive current density value of almost 15 mA cm^{-2} (see Table 2), recorded at the equilibrium water oxidation potential, and exhibited a photocurrent at ca. 1.7 mA cm^{-2} (350 W Xenon lamp, 100 mW cm^{-2}) while it also presented noteworthy current stability with practically no losses for 10000 s.

Considering the previous works as steppingstones and hereafter focusing solely on the role of WS_2, a system of exfoliated WS_2 nanosheets deposited onto WO_3 nanoplates, aiming to form another type II heterojunction for PEC water splitting, was investigated.[109] The system was probed in neutral pH conditions (aqueous 0.5 M Na_2SO_4 electrolyte) under illumination (300 W Xenon lamp, 100 mW cm^{-2}). Notably, WO_3 possesses an impressive bandgap (2.5–2.8 eV) for photo-related applications, yet it suffers from weak absorption at the visible region and short hole diffusion lengths. When W foil is oxidized to WO_3, onto that LPE-produced WS_2 nanosheets were deposited, followed by calcination (at either 90 or 450 °C), a type II heterojunction was formed. The WO_3-WS_2 photoanode formed at 450 °C, presented 7 times higher generated photocurrent compared to bare WO_3. This behavior is ascribed to WS_2 catalyzing OER, while mechanistically speaking, holes are transferred from WO_3 to WS_2 and electrons from the valence band of WS_2 to the conduction band of WO_3 (**Figure 8**). Reduced charge recombination observed via transient studies, better conductivity profile (lower charge transfer resis-

tance) and appreciable photon-to-current conversion (increased IPCE), indicated the superiority of this system (see Table 2).

Another heterojunction that was furnished upon combination of hematite α-Fe_2O_3 and WS_2 was examined.[110] Specifically, exfoliated WS_2 nanosheets were dropcasted onto the hematite film on FTO glass and calcined at 450 °C to form protective ionic oxide forms of WS_2 (WO_x: WO_3^-, WO^+, etc.). The α-$Fe_2O_3/WS_2/WO_x$ hybrid, in the form of core-shell nanorods, exhibited a 14 and 30-times higher than bare hematite rapid and constant anodic photocurrent, instantaneously when illuminated from either WS_2/WO_x side or FTO side (0.98 and 0.21*vs.* 0.07 mA cm^{-2}, respectively), in aqueous 1.0 M NaOH electrolyte, using a solar simulator as the light source (300 W Xe lamp, 100 mW cm^{-2}). The WS_2/WO_x adds to the system by offering more oxygen vacancies and ionic forms that facilitate charge transfer. The α-$Fe_2O_3/WS_2/WO_x$ hybrid is characterized by increased absorption at the Vis region, higher exciton lifetimes and more charge carriers, which are equal to increased conductivity. All the above were confirmed by the high IPCE value of α-$Fe_2O_3/WS_2/WO_x$ (15.5%*vs.* 1.65% of pure hematite), 50% higher than hematite double layer capacitance, which leads to increased **ECSA** and lower R_{ct} value (see Table 2).

Fabrication of a 3D photoanode consisting of hydrothermally grown TiO_2 nanoarrays (NAs) onto FTO substrate and subsequent coating with Li-assisted exfoliated mixed-phase WS_2 was developed, targeting PEC of kinetically impeded water oxidation.[111] 1T-WS_2 nanosheets, occupying more than 55% of the mixture, offer better charge separation and electron transport at the interfacial region. This system was tested in neutral pH conditions (aqueous 0.5 M Na_2SO_4 solution), under illumination (1 sun, AM 1.5G). The TiO_2 NAs-WS_2 photoelectrode demonstrated more than 50% elevated photocurrent at 570 mV of overpotential (1.8 mA cm^{-2}) compared to bare TiO_2 (0.8 mA cm^{-2}) and a three-fold increased solar energy conversion efficiency at a bias potential, again versus individual TiO_2 (0.09% *vs.* 0.03%). The better photo-electrocatalytic profile was ascribed to accelerated charge transport, mainly driven by the highly metallic character of WS_2 (see Table 2). Another reason could be induced hole migration to WS_2 surface, where oxidation of water is facilitated, corroborated by 40% lowered R_{ct} of the hybrid system (1081 *vs.* 1811 Ω).

In the field of non-PEC applications, colloidally synthesized, followed by Li-assisted exfoliation, 1T-WS_2 nanosheets decorated with Ni moieties, exhibited interesting anodic current.[112] Ni cations were introduced at percentages varying from 9 to 47% with respect to W atoms, anchoring to introduced sulfide anion groups, eventually leading to dispersed Ni moieties, covalently bound to the tethered sulfides. Electrochemically, in aqueous 0.1 M KOH solution, systems with highly dispersed Ni atoms had high intrinsic activity and demonstrated better results on water oxidation reaction, whereas lower dispersion of Ni created clusters that reduced catalyst activity due to active site blockage. The Ni-doped system, compared to 1T- Li_xWS_y as well as to control sample $Ni(OH)_2$, exhibited 200 and 20-fold greater current densities, respectively (see Table 1).

In another work involving Ni moieties, WS_2 nanorods built on Ni backbone, led to an efficient OER electrocatalyst.[113] Cetyltrimethylammonium bromide (CTAB)-mediated LPE produced WS_2 nanosheets onto that Ni_2O_3 particles were grown (WS_2-Ni_2O_3), were thermally treated under reductive conditions to convert Ni oxide particles to metal Ni^0 particles, that served as the scaffold to realize Ni-containing WS_2 nanorods (WS_2-r). The WS_2-Ni_2O_3 and WS_2-r with Ni content ≈18% and 14%, respectively, were assayed in aqueous 1.0 M KOH electrolyte and found to exhibit lower than RuO_2 η_{10} values (370 mV, 334 mV and 381 mV for WS_2-Ni_2O_3, WS_2-r and RuO_2, respectively). Clearly exploiting the synergy between WS_2 and dispersed Ni active centers, in terms of impedance, WS_2-r exhibited the lowest R_{ct} (2.2 Ohm) while the same material was characterized by remarkable stability (3% voltage drop at 10 mA cm^{-2} over the course of 10 h), highlighting its overall excellent performance (see Table 1).

In a recent work of our research group, exfoliated 2H-WS_2 nanosheets were interfaced via covalent linkage with OER active Ni-porphyrin moieties through rational design, aiming for superior OER catalytic activity in aqueous electrolyte (**Figure 9**).[114] Lipoic acid-based, Ni-porphyrin derivatives were attached onto S-vacant sites of WS_2 nanosheet edges via dithiolane linkages, leading to a functionalized nanohybrid (WS_2-NiP). Interestingly, WS_2-NiP presented a competitive OER electroactivity, surpassing both its precursors as well as RuO_2 (see Table 1). Since both exfoliated WS_2 nanosheets as well as the non-metalated porphyrin hybrid counterpart (WS_2-H_2P) exhibited no sign of activity whatsoever, the essence of OER activity stems from Ni centers and the through-space communication with the TMD lattice. The low Tafel slope and lower than RuO_2 charge transfer resistance, render this system a promising scaffold for realistic electrode fabrication. Moreover, due to photoactivity of porphyrin moieties, illumination of WS_2-NiP hybrid led to photocurrent evolution, 10 times higher than that of WS_2-H_2P, proving that the nanohybrid could also function in PEC applications.

3.3. $MoSe_2$ as Electrocatalyst for Water Oxidation

Transition metal selenides are equivalent of sulfides in terms of structure, yet they facilitate electron transfer owing to their higher intrinsic conductivity. The latter is attributed to the greater metallic character of Se compared to S and to its electronic structure ($4s^2$ $4p^4$). This kind of orbital filling allows Se to easily draw two electrons and form Se^{2-} anions, while having an empty 3d orbital in the valence shell encourages bonding to d orbital bearing metals.[115]

However, only a few works exist that examine exfoliated $MoSe_2$ capabilities in OER. Specifically, a heterostructure through combination of H_2O_2-assisted LPE produced $MoSe_2$ flakes, Mo_2C and SWNTs was formulated (**Figure 10**).[116] By filtering dispersions of either $MoSe_2$ or $MoSe_2$-Mo_2C mixture on a membrane containing pre-filtered SWNTs, the composites were realized. Different concentrations of H_2O_2 per volume (0.1%–0.3%) led to nanopore-rich (prepared through chemical etching) nanosheets, different in terms of thickness and lateral dimension and with negligible metal oxide presence. H_2O_2 at 0.2% was found to be the ideal quantity used, where smaller dimensions of $MoSe_2$ nanoflakes, in the absence of aggregates, were furnished. Regarding OER, poor activity was recorded in acidic conditions, whereas in alkaline conditions, $MoSe_2/Mo_2C$ presented interesting results and when SWNTs were introduced, the

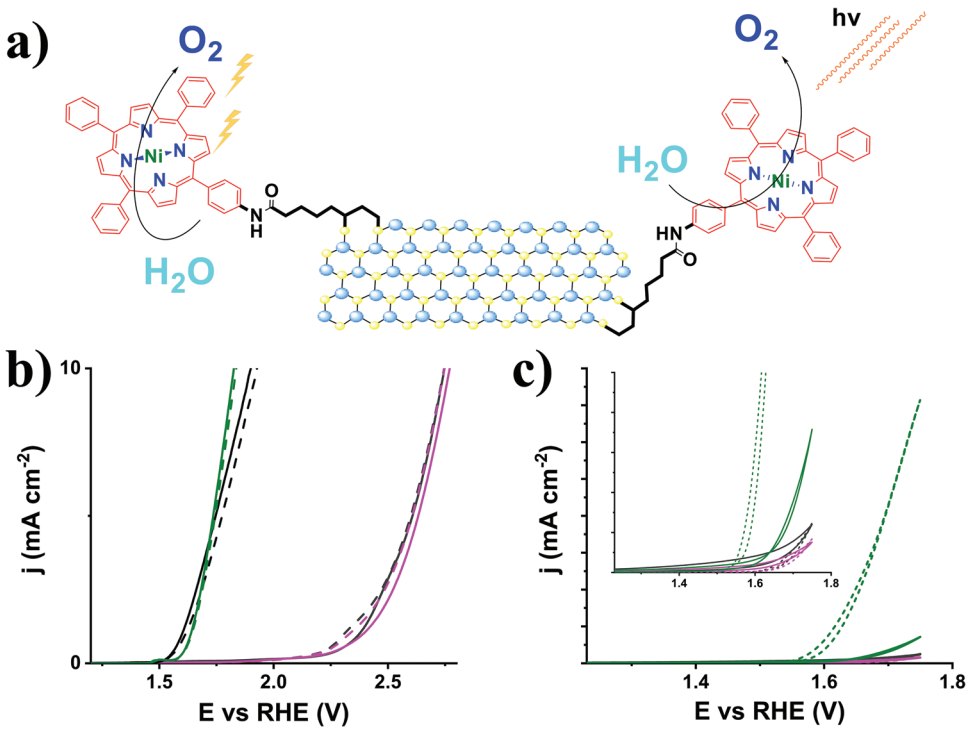

Figure 9. a) Schematic illustration of WS_2-NiP hybrid nanomaterial, active on water oxidation under application of external voltage or illumination, b) linear sweep voltammograms (LSVs) of WS_2 nanosheets (dark gray), WS_2-H_2P (magenta), RuO_2 (black) and WS_2-NiP (olive) in 0.1 M KOH electrolyte for water oxidation and c) cyclic voltammograms (CVs) of WS_2 nanosheets (dark gray), WS_2-H_2P (magenta) and WS_2-NiP (olive) under illumination (150 W Xe lamp, 100 mW cm^{-2}). Reproduced with permission.[114] Copyright 2023, Wiley-VCH GmbH.

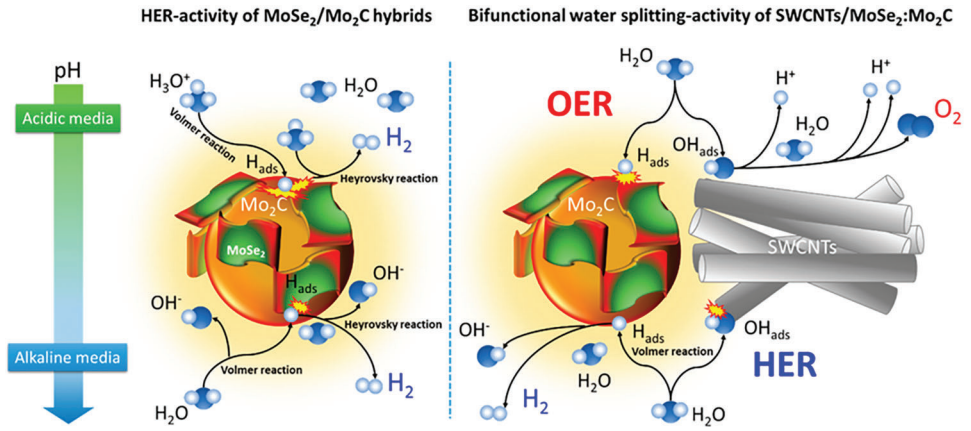

Figure 10. Schematic representation of $MoSe_2/Mo_2C$/SWNTs nanohybrid. Synergetic effects trigger the bifunctionality of the system, transforming it from a sole HER catalyst (left side) to a water splitting catalyst (right side). Reproduced with permission.[116] Copyright 2019, American Chemical Society.

SWNTs/$MoSe_2$/Mo_2C hybrid was characterized by bifunctionality. The latter heterostructure presented tantamount to the benchmark IrO_2/RuO_2 anodic η_{10} values of 0.197 and 0.241 V in acidic and alkaline conditions, respectively (see Table 1). Even though the nanoporous structure of $MoSe_2$ possibly worked protectively against mechanical damage from produced hydrogen bubbles, an expected degradation process in anodic currents took place, possibly attributed to carbon oxidation of single-walled carbon nanotubes (SWCNTs) and detachment from the heterostructure. Eventually, this led to almost 50% current density loss in the first 30 min, in both conditions.

In another work, the influence of first-row transition metals (Co, Ni) in their nanoparticle form on OER activity of $MoSe_2$ was investigated. A structure with both metals Co and Ni as nanoparticles was formed, which aided both the exfoliation of bulk $MoSe_2$, to realize its few-layered counterpart and produced the corresponding NPs in situ onto the $MoSe_2$ lattice via sonication and thermal treatment.[117] In a uniformly decorated surface,

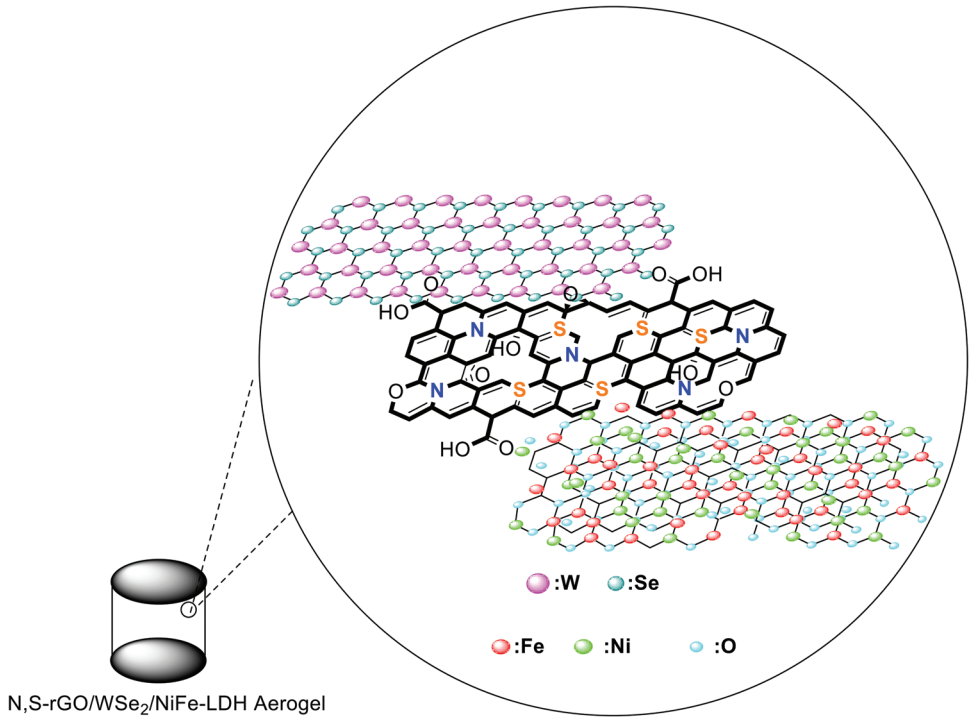

Figure 11. Schematic illustration of the N,S-rGO/WSe_2/NiFe-LDH aerogel nanostructure.[120]

synergy between conductive $MoSe_2$ lattice and metal centers that behave as active sites, a missing OER feature of $MoSe_2$ basal plane, did present some interesting results. Every material, namely $MoSe_2$ decorated with only Co, only Ni and with both metals, was tested in aqueous 1.0 M KOH solution. $MoSe_2$-Ni exhibited the lowest η_{10} value (see Table 1) versus the 380 mV of RuO_2 and a 50% lowered R_{ct} (3.1 *vs.* 6.4 Ohm), while in terms of kinetics, $MoSe_2$-Co showed a Tafel slope of 109 mV dec^{-1}, lower than RuO_2 (136 mV dec^{-1}). Even though $MoSe_2$-CoNi did not present the best results among all screened materials, it still possessed characteristics that match those of RuO_2 (η_{10} = 378 mV, Tafel slope = 170 mV dec^{-1} and R_{ct} = 4 Ohm). These materials were also active in HER, which consequently highlights their potential for overall WS, a fact further supported by the observed stability, where no overpotential changes occurred while applying chronopotentiometry at 10 mA cm^{-2} for 10 h.

3.4. WSe_2 as Electrocatalyst for Water Oxidation

Very little work has been done on exfoliated WSe_2 interfacing OER active elements. Nanohybrid dots (NHDs) of WSe_2-CdS with ultra-small diameter (2-3 nm) as potential bifunctional ORR/OER electrocatalyst were prepared.[118] The LPE-produced nanosheets were converted to NHDs via a sonication-centrifugation-dialysis process. All prepared materials were screened against ORR and OER, where WSe_2-CdS was found to perform marginally better than benchmark Pt/C and RuO_2 catalysts. In fact, WSe_2-CdS showed a superior profile in both reactions, in terms of electrochemical characteristics, which can be ascribed to the small size of NHDs (see Table 1). This hybrid is very close to the ideal reversible oxygen electrode with the reason being the synergistic effects taking place at the WSe_2-CdS interface.[119] The large surface area and the higher number of exposed edges, which originate from the nanoscale sizes as well as the presence of CdS, which also functions as a means of preventing aggregation, are responsible for the astounding electrocatalytic profile of these materials.

With an aim to rationally design an effective electrocatalyst, a super-structure of 3D N,S-doped reduced graphene oxide (rGO) decorated with WSe_2 and NiFe-LDH nanosheets was conceptualized and prepared as a potential overall WS catalyst (**Figure 11**).[120] Such a structure was realized by incorporating exfoliated WSe_2 onto N, S-co-doped graphene, under solvothermal conditions and immersing the product into the exfoliated NiFe-LDH dispersion to complete the formation of the composite. The 3D framework exhibited an anodic η_{10} value of 250 and 360 mV to achieve 10 and 100 mA cm^{-2} current density values, very close to the equivalent values for RuO_2 (see Table 1). Additionally, the composite also presented noticeable HER activity, thus proving that the catalytic strength in different reactions of each individual element, is transferred to the final nano ensemble. The synergetic effects stemming from inter-layer communication are the main reason for the sharing of electrocatalytic elements. The WSe_2-NiFe-LDH-N,S-codoped rGO electrocatalyst was also proved to be durable at voltages below 1.8 V versus RHE over the course of 10 h, exhibiting robustness. The ample nanoporous surface, which renders active sites more easily accessible and the N, S-doping on rGO surface, that increases the conductivity and facilitates rapid charge transfer between the active sites and the electrolyte, form the basis for the excellent electrocatalytic activity of this nanocomposite bifunctional catalyst.

Collectively, all the above results from each of these different works are summarized in Table 1 and Table 2, where the latter is dedicated to hybrid materials involved in photo-electrocatalytic applications. Even though a low amount of works about exfoliated TMDs as core part of OER electrocatalytic systems exists, it is apparent that that the previous 5 years there has been a surge in such new works. Consequently, this field of subject is currently in a growth phase, and it is expected that it will soon occupy the front stage of OER catalyzing systems.

4. Summary and Perspectives

In the field of water splitting devices, TMOs are the electrocatalyst species closer than any other to finally reaching an adequate for industrial standards TRL. That has also been proved by the fact that they have already been used for practical applications, namely perovskite oxides in photovoltaics. However, it is also apparent that TMOs have significant weaknesses, as mentioned above, and research teams worldwide need to shift their attention to TMPs, TMNs and more specifically to TMDs. In view of all the works presented in this review, it has been proved that TMDs are characterized by high applicability and combination with different electroactive elements is quite facile. Specifically, they presented remarkable flexibility in chemical functionalization, heterostructure assembly, nanoparticle stabilization and heterojunction formation, to name but a few. Additionally, and probably most importantly, they are also easily tunable in terms of bandgap, defect, and phase engineering, all with the effective exfoliation tactics. More research, both on laboratory scale and industrial level is encouraged to decide on which combination of exfoliation elements (solvent, conditions, agitation method) is the most beneficial for mass production so that attention will be shifted there. Furthermore, as presented both in this work and in the TMD literature in general, TMD-based systems almost always exhibit bi- or even tri-functional character meaning that both anode and cathode can be formulated with the same material. Subsequently, this can lead to a "universal" electrode for electrolyzer applications, reducing the overall cost of perfecting anode and cathode electrodes separately. Overall, the positive elements that TMDs can offer along with the dynamics of exfoliation as a technique easily adjustable to industry standards, can put TMD-based hybrids on the way to rapidly being incorporated by the industry. Gazing at the big picture, in the perfection of an OER electrocatalyst as a whole, swiftly developing A.I. systems can significantly aid this venture. By acquiring the distillate of all OER-relevant literature, processed by A.I., the characteristics that are pivotal for such activity can be summarized and by running multiple DFT calculations on what makes each newly reported OER electrocatalyst effective, the top aspects of this kind of electroactivity can be further incorporated in the most promising scaffold.

Conflict of Interest

The authors declare no conflict of interest.

Author Contributions

N.T. conceived the concept. M.P.M. and N.T. co-wrote the manuscript. All authors participated in manuscript discussion.

Keywords

electrocatalysts, hydrogen, oxygen evolution reaction, transition metal dichalcogenides, water splitting

Received: May 8, 2023
Revised: June 21, 2023
Published online: July 17, 2023

[1] I. Dincer, *Int. J. Hydrogen Energy* **2012**, *37*, 1954.
[2] A. Ursua, L. M. Gandia, P. Sanchis, *Proc. IEEE* **2012**, *100*, 410.
[3] S. Koumi Ngoh, D. Njomo, *Renewable Sustainable Energy Rev.* **2012**, *16*, 6782.
[4] D.-Y. Lee, A. Elgowainy, Q. Dai, *Appl. Energy* **2018**, *217*, 467.
[5] N. Du, C. Roy, R. Peach, M. Turnbull, S. Thiele, C. Bock, *Chem. Rev.* **2022**, *122*, 11830.
[6] V. Vij, S. Sultan, A. M. Harzandi, A. Meena, J. N. Tiwari, W.-G. Lee, T. Yoon, K. S. Kim, *ACS Catal.* **2017**, *7*, 7196.
[7] J. Li, G. Zheng, *Adv. Sci.* **2017**, *4*, 1600380.
[8] M. Fang, G. Dong, R. Wei, J. C. Ho, *Adv. Energy Mater.* **2017**, *7*, 1700559.
[9] Q. Liang, G. Brocks, A. Bieberle-Hütter, *J. Phys. Energy* **2021**, *3*, 026001.
[10] J. C. Fornaciari, L.-C. Weng, S. M. Alia, C. Zhan, T. A. Pham, A. T. Bell, T. Ogitsu, N. Danilovic, A. Z. Weber, *Electrochim. Acta* **2022**, *405*, 139810.
[11] W. Li, C. Wang, X. Lu, *J. Mater. Chem. A* **2021**, *9*, 3786.
[12] J. Song, C. Wei, Z.-F. Huang, C. Liu, L. Zeng, X. Wang, Z. J. Xu, *Chem. Soc. Rev.* **2020**, *49*, 2196.
[13] X. Xie, L. Du, L. Yan, S. Park, Y. Qiu, J. Sokolowski, W. Wang, Y. Shao, *Adv. Funct. Mater.* **2022**, *32*, 2110036.
[14] S. Chu, A. Majumdar, *Nature* **2012**, *488*, 294.
[15] Y. Jiao, Y. Zheng, M. Jaroniec, S. Z. Qiao, *Chem. Soc. Rev.* **2015**, *44*, 2060.
[16] D. A. J. Rand, *J. Solid State Electrochem.* **2011**, *15*, 1579.
[17] M. Bodner, A. Hofer, V. Hacker, *Wiley Interdiscip. Rev. Energy Environ.* **2015**, *4*, 365.
[18] P. Zhang, L. Yu, X. W. (David) Lou, *Angew. Chem. Int. Ed. Engl.* **2018**, *57*, 15076.
[19] P. Zhang, X. F. Lu, J. Nai, S. Zang, X. W. (David) Lou, *Adv. Sci.* **2019**, *6*, 1900576.
[20] S. Dresp, F. Luo, R. Schmack, S. Kühl, M. Gliech, P. Strasser, *Energy Environ. Sci.* **2016**, *9*, 2020.
[21] X. F. Lu, Y. Chen, S. Wang, S. Gao, X. W. (David) Lou, *Adv. Mater.* **2019**, *31*, 1902339.
[22] M. Zhang, Q. Dai, H. Zheng, M. Chen, L. Dai, *Adv. Mater.* **2018**, *30*, 1705431.
[23] Z. Chen, L. Guo, L. Pan, T. Yan, Z. He, Y. Li, C. Shi, Z. Huang, X. Zhang, J. Zou, *Adv. Energy Mater.* **2022**, *12*, 2103670.
[24] X. Lu, C. Zhao, *Nat. Commun.* **2015**, *6*, 6616.
[25] T. Su, Q. Shao, Z. Qin, Z. Guo, Z. Wu, *ACS Catal.* **2018**, *8*, 2253.
[26] C. Wang, L. Jin, H. Shang, H. Xu, Y. Shiraishi, Y. Du, *Chinese Chem. Lett.* **2021**, *32*, 2108.
[27] H. Yu, J. Ge, *Curr. Opin. Electrochem.* **2023**, 101296.
[28] J. Su, Y. Yang, G. Xia, J. Chen, P. Jiang, Q. Chen, *Nat. Commun.* **2017**, *8*, 14969.
[29] J. P. Hughes, J. Clipsham, H. Chavushoglu, S. J. Rowley-Neale, C. E. Banks, *Renewable Sustainable Energy Rev.* **2021**, *139*, 110709.
[30] K. Zeng, D. Zhang, *Prog. Energy Combust. Sci.* **2010**, *36*, 307.
[31] Y. Li, Y. Sun, Y. Qin, W. Zhang, L. Wang, M. Luo, H. Yang, S. Guo, *Adv. Energy Mater.* **2020**, *10*, 1903120.
[32] H. Adamu, S. I. Abba, P. B. Anyin, Y. Sani, Z. H. Yamani, M. Qamar, *ACS Mater. Lett.* **2023**, *5*, 299.

[33] D. K. Perivoliotis, J. Ekspong, X. Zhao, G. Hu, T. Wågberg, E. Gracia-Espino, *Nano Today* **2023**, *50*, 101883.
[34] P. Li, R. Zhao, H. Chen, H. Wang, P. Wei, H. Huang, Q. Liu, T. Li, X. Shi, Y. Zhang, M. Liu, X. Sun, *Small* **2019**, *15*, 1805103.
[35] Y. Luo, Z. Zhang, M. Chhowalla, B. Liu, *Adv. Mater.* **2022**, *34*, 2108133.
[36] L. Tian, Y. Liu, C. He, S. Tang, J. Li, Z. Li, *Chem. Rec.* **2023**, *23*, e202200213.
[37] Y. S. Jeong, J.-B. Park, H.-G. Jung, J. Kim, X. Luo, J. Lu, L. Curtiss, K. Amine, Y.-K. Sun, B. Scrosati, Y. J. Lee, *Nano Lett.* **2015**, *15*, 4261.
[38] J. Creus, J. De Tovar, N. Romero, J. García-Antón, K. Philippot, R. Bofill, X. Sala, *ChemSusChem* **2019**, *12*, 2493.
[39] F. Bizzotto, J. Quinson, A. Zana, J. J. K. Kirkensgaard, A. Dworzak, M. Oezaslan, M. Arenz, *Catal. Sci. Technol.* **2019**, *9*, 6345.
[40] A. R. Poerwoprajitno, L. Gloag, T. M. Benedetti, S. Cheong, J. Watt, D. L. Huber, J. J. Gooding, R. D. Tilley, *Small* **2019**, *15*, 1804577.
[41] D. Böhm, M. Beetz, C. Gebauer, M. Bernt, J. Schröter, M. Kornherr, F. Zoller, T. Bein, D. Fattakhova-Rohlfing, *Appl. Mater. Today* **2021**, *24*, 101134.
[42] K. Zeng, X. Zheng, C. Li, J. Yan, J. Tian, C. Jin, P. Strasser, R. Yang, *Adv. Funct. Mater.* **2020**, *30*, 2000503.
[43] Z. Li, P. Wei, G. Wang, *Energy Fuels* **2022**, *36*, 11724.
[44] Z. Yu, Y. Bai, G. Tsekouras, Z. Cheng, *Nano Sel.* **2022**, *3*, 766.
[45] B. M. Hunter, W. Hieringer, J. R. Winkler, H. B. Gray, A. M. Müller, *Energy Environ. Sci.* **2016**, *9*, 1734.
[46] W.-D. Zhang, H. Yu, T. Li, Q.-T. Hu, Y. Gong, D.-Y. Zhang, Y. Liu, Q.-T. Fu, H.-Y. Zhu, X. Yan, Z.-G. Gu, *Appl. Catal. B* **2020**, *264*, 118532.
[47] W.-D. Zhang, Q.-T. Hu, L.-L. Wang, J. Gao, H.-Y. Zhu, X. Yan, Z.-G. Gu, *Appl. Catal. B* **2021**, *286*, 119906.
[48] Y. Liu, Y. Wang, S. Zhao, Z. Tang, *Small Methods* **2022**, *6*, 2200773.
[49] A. H. Al-Naggar, N. M. Shinde, J.-S. Kim, R. S. Mane, *Coord. Chem. Rev.* **2023**, *474*, 214864.
[50] Y. Guo, T. Park, J. W. Yi, J. Henzie, J. Kim, Z. Wang, B. Jiang, Y. Bando, Y. Sugahara, J. Tang, Y. Yamauchi, *Adv. Mater.* **2019**, *31*, 1807134.
[51] M. Chhowalla, H. S. Shin, G. Eda, L.-J. Li, K. P. Loh, H. Zhang, *Nat. Chem.* **2013**, *5*, 263.
[52] X. Chia, A. Y. S. Eng, A. Ambrosi, S. M. Tan, M. Pumera, *Chem. Rev.* **2015**, *115*, 11941.
[53] S. Manzeli, D. Ovchinnikov, D. Pasquier, O. V. Yazyev, A. Kis, *Nat. Rev. Mater.* **2017**, *2*, 17033.
[54] N. Huo, Y. Yang, J. Li, *J. Semicond.* **2017**, *38*, 031002.
[55] C. Tsai, F. Abild-Pedersen, J. K. Nørskov, *Nano Lett.* **2014**, *14*, 1381.
[56] X. Duan, J. Xu, Z. Wei, J. Ma, S. Guo, H. Liu, S. Dou, *Small Methods* **2017**, *1*, 1700156.
[57] A. Mondal, A. Vomiero, *Adv. Funct. Mater.* **2022**, 2208994.
[58] A. K. Mishra, K. V. Lakshmi, L. Huang, *Sci. Rep.* **2015**, *5*, 15718.
[59] S. Choi, K. C. Kwon, S. Y. Kim, H. W. Jang, *FlatChem* **2017**, *4*, 68.
[60] J. N. Coleman, M. Lotya, A. O'neill, S. D. Bergin, P. J. King, U. Khan, K. Young, A. Gaucher, S. De, R. J. Smith, I. V Shvets, S. K. Arora, G. Stanton, H.-Y. Kim, K. Lee, G. T. Kim, G. S. Duesberg, T. Hallam, J. J. Boland, J. J. Wang, J. F. Donegan, J. C. Grunlan, G. Moriarty, A. Shmeliov, R. J. Nicholls, J. M. Perkins, E. M. Grieveson, K. Theuwissen, D. W. Mccomb, P. D. Nellist, et al., *Science* **2011**, *331*, 568.
[61] M. Wang, L. Zhang, Y. He, H. Zhu, *J. Mater. Chem. A* **2021**, *9*, 5320.
[62] Q. Zhang, L. Mei, X. Cao, Y. Tang, Z. Zeng, *J. Mater. Chem. A* **2020**, *8*, 15417.
[63] S. Chandrasekaran, D. Ma, Y. Ge, L. Deng, C. Bowen, J. Roscow, Y. Zhang, Z. Lin, R. D. K. Misra, J. Li, P. Zhang, H. Zhang, *Nano Energy* **2020**, *77*, 105080.
[64] P. Joensen, R. F. Frindt, S. R. Morrison, *Mater. Res. Bull.* **1986**, *21*, 457.
[65] K.-G. Zhou, N.-N. Mao, H.-X. Wang, Y. Peng, H.-L. Zhang, *Angew. Chem. Int. Ed.* **2011**, *123*, 11031.
[66] R. J. Smith, P. J. King, M. Lotya, C. Wirtz, U. Khan, S. De, A. O'Neill, G. S. Duesberg, J. C. Grunlan, G. Moriarty, J. Chen, J. Wang, A. I. Minett, V. Nicolosi, J. N. Coleman, *Adv. Mater.* **2011**, *23*, 3944.
[67] V. Nicolosi, M. Chhowalla, M. G. Kanatzidis, M. S. Strano, J. N. Coleman, *Science* **2013**, *340*, 72.
[68] Z. Lin, Y. Liu, U. Halim, M. Ding, Y. Liu, Y. Wang, C. Jia, P. Chen, X. Duan, C. Wang, F. Song, M. Li, C. Wan, Y. Huang, X. Duan, *Nature* **2018**, *562*, 254.
[69] S. Biccai, S. Barwich, D. Boland, A. Harvey, D. Hanlon, N. McEvoy, J. N. Coleman, *2D Mater.* **2018**, *6*, 015008.
[70] Z. Lin, Z. Wan, F. Song, B. Huang, C. Jia, Q. Qian, J. S. Kang, Y. Wu, X. Yan, L. Peng, C. Wan, J. Zhou, Z. Sofer, I. Shakir, Z. Almutairi, S. Tolbert, X. Pan, Y. Hu, Y. Huang, X. Duan, *Chem* **2021**, *7*, 1887.
[71] H. Lin, J. Wang, Q. Luo, H. Peng, C. Luo, R. Qi, R. Huang, J. Travas-Sejdic, C.-G. Duan, *J. Alloys Compd.* **2017**, *699*, 222.
[72] G. Pagona, C. Bittencourt, R. Arenal, N. Tagmatarchis, *Chem. Commun.* **2015**, *51*, 12950.
[73] E. P. Nguyen, B. J. Carey, J. Z. Ou, J. van Embden, E. Della Gaspera, A. F. Chrimes, M. J. S. Spencer, S. Zhuiykov, K. Kalantar-zadeh, T. Daeneke, *Adv. Mater.* **2015**, *27*, 6225.
[74] M. Jeong, S. Kim, S.-Y. Ju, *RSC Adv.* **2016**, *6*, 36248.
[75] R. Canton-Vitoria, Y. Sayed-Ahmad-Baraza, M. Pelaez-Fernandez, R. Arenal, C. Bittencourt, C. P. Ewels, N. Tagmatarchis, *npj 2D Mater. Appl.* **2017**, *1*, 13.
[76] D. Voiry, A. Goswami, R. Kappera, C. D. C. C. E. Silva, D. Kaplan, T. Fujita, M. Chen, T. Asefa, M. Chhowalla, *Nat. Chem.* **2015**, *7*, 45.
[77] K. C. Knirsch, N. C. Berner, H. C. Nerl, C. S. Cucinotta, Z. Gholamvand, N. McEvoy, Z. Wang, I. Abramovic, P. Vecera, M. Halik, S. Sanvito, G. S. Duesberg, V. Nicolosi, F. Hauke, A. Hirsch, J. N. Coleman, C. Backes, *ACS Nano* **2015**, *9*, 6018.
[78] D. Voiry, M. Salehi, R. Silva, T. Fujita, M. Chen, T. Asefa, V. B. Shenoy, G. Eda, M. Chhowalla, *Nano Lett.* **2013**, *13*, 6222.
[79] M. Stavrou, N. Chazapis, E. Nikoli, R. Arenal, N. Tagmatarchis, S. Couris, *ACS Appl. Nano Mater.* **2022**, *5*, 16674.
[80] T. Shaker, H. Mehdipour, A. Z. Moshfegh, *Int. J. Hydrogen Energy* **2022**, *47*, 1579.
[81] P. M. Pataniya, C. K. Sumesh, *Appl. Surf. Sci.* **2021**, *563*, 150323.
[82] Q. D. Truong, Y. Nakayasu, Q. T. Nguyen, D. N. Nguyen, C. T. Nguyen, M. K. Devaraju, D. Rangappa, K. Nayuki, Y. Sasaki, P. D. Tran, T. Tomai, I. Honma, *Appl. Surf. Sci.* **2020**, *505*, 144537.
[83] P. M. Pataniya, X. Yang, B. Li, D. Kannichankandy, C. K. Sumesh, *Int. J. Energy Res.* **2022**, *46*, 12073.
[84] E. German, R. Gebauer, *Appl. Surf. Sci.* **2020**, *528*, 146591.
[85] S. Anantharaj, K. Karthick, S. Kundu, *Mater. Today Energy* **2017**, *6*, 1.
[86] S. Anantharaj, S. R. Ede, K. Karthick, S. Sam Sankar, K. Sangeetha, P. E. Karthik, S. Kundu, *Energy Environ. Sci.* **2018**, *11*, 744.
[87] D. Xiong, Q. Zhang, W. Li, J. Li, X. Fu, M. F. Cerqueira, P. Alpuim, L. Liu, *Nanoscale* **2017**, *9*, 2711.
[88] K. Hu, J. Zhou, Z. Yi, C. Ye, H. Dong, K. Yan, *Appl. Surf. Sci.* **2019**, *465*, 351.
[89] Z. Chen, W. Wang, S. Huang, P. Ning, Y. Wu, C. Gao, T.-T. Le, J. Zai, Y. Jiang, Z. Hu, X. Qian, *Nanoscale* **2020**, *12*, 326.
[90] M. Muska, J. Yang, Y. Sun, J. Wang, Y. Wang, Q. Yang, *ACS Appl. Nano Mater.* **2021**, *4*, 5796.
[91] J. Wu, M. Liu, K. Chatterjee, K. P. Hackenberg, J. Shen, X. Zou, Y. Yan, J. Gu, Y. Yang, J. Lou, P. M. Ajayan, *Adv. Mater. Interfaces* **2016**, *3*, 1500669.
[92] S. Li, Z. Zhao, D. Yu, J.-Z. Zhao, Y. Su, Y. Liu, Y. Lin, W. Liu, H. Xu, Z. Zhang, *Nano Energy* **2019**, *66*, 104083.
[93] T. Rao, H. Wang, Y. Zeng, Z. Guo, H. Zhang, W. Liao, *Adv. Sci.* **2021**, *8*, 2002284.
[94] Z. Sadighi, J. Liu, L. Zhao, F. Ciucci, J.-K. Kim, *Nanoscale* **2018**, *10*, 22549.

[95] W.-J. Kwak, Rosy, D. Sharon, C. Xia, H. Kim, L. R. Johnson, P. G. Bruce, L. F. Nazar, Y.-K. Sun, A. A. Frimer, M. Noked, S. A. Freunberger, D. Aurbach, *Chem. Rev.* **2020**, *120*, 6626.
[96] B. Lai, S. C. Singh, J. K. Bindra, C. S. Saraj, A. Shukla, T. P. Yadav, W. Wu, S. A. McGill, N. S. Dalal, A. Srivastava, C. Guo, *Mater Today Chem* **2019**, *14*, 100207.
[97] I. M. Sadiek, A. M. Mohammad, M. E. El-Shakre, M. S. El-Deab, *Int. J. Hydrogen Energy* **2012**, *37*, 68.
[98] L. Lei, D. Huang, C. Lai, C. Zhang, R. Deng, Y. Chen, S. Chen, W. Wang, *J. Mater. Chem. A* **2020**, *8*, 15074.
[99] Y. Li, Z. Yin, X. Liu, M. Cui, S. Chen, T. Ma, *Mater Today Chem* **2021**, *19*, 100411.
[100] J. Cai, X. Zhang, Y. Pan, Y. Kong, S. Lin, *Int. J. Hydrogen Energy* **2021**, *46*, 34252.
[101] L. Yang, H. Qi, C. Zhang, X. Sun, *Nanotechnology* **2016**, *27*, 23LT01.
[102] P. Ferreira, B. Abreu, C. Freire, D. M. Fernandes, E. F. Marques, *Materials* **2021**, *14*, 896.
[103] P. Xiong, X. Zhang, H. Wan, S. Wang, Y. Zhao, J. Zhang, D. Zhou, W. Gao, R. Ma, T. Sasaki, G. Wang, *Nano Lett.* **2019**, *19*, 4518.
[104] R. Prasannachandran, T. V. Vineesh, M. B. Lithin, R. Nandakishore, M. M. Shaijumon, *Chem. Commun.* **2020**, *56*, 8623.
[105] Y. S. Cho, D. Rhee, H. J. Kim, H. S. Kim, J. M. Baik, J. Kang, *Adv. Mater. Interfaces* **2021**, *8*, 2101576.
[106] C.-B. Sun, Y.-W. Zhong, W.-J. Fu, Z.-Q. Zhao, J. Liu, J. Ding, X.-P. Han, Y.-D. Deng, W.-B. Hu, C. Zhong, *Tungsten* **2020**, *2*, 109.
[107] F. M. Pesci, M. S. Sokolikova, C. Grotta, P. C. Sherrell, F. Reale, K. Sharda, N. Ni, P. Palczynski, C. Mattevi, *ACS Catal.* **2017**, *7*, 4990.
[108] M. Mojaddami, A. Simchi, *Renew. Energy* **2020**, *162*, 504.
[109] M. Tayebi, Z. Masoumi, B.-K. Lee, *Ultrason. Sonochem.* **2021**, *70*, 105339.
[110] Z. Masoumi, M. Tayebi, M. Kolaei, B.-K. Lee, *Appl. Catal. B* **2022**, *313*, 121447.
[111] Y. Pi, B. Liu, Z. Li, Y. Zhu, Y. Li, F. Zhang, G. Zhang, W. Peng, X. Fan, *J. Colloid Interface Sci.* **2019**, *545*, 282.
[112] E. Meza, R. E. Diaz, C. W. Li, *ACS Nano* **2020**, *14*, 2238.
[113] K. Maslana, K. Wenelska, M. Biegun, E. Mijowska, *Appl. Catal. B* **2020**, *266*, 118575.
[114] M. P. Minadakis, R. Canton-Vitoria, C. Stangel, E. Klontzas, R. Arenal, J. Hernández-Ferrer, A. M. Benito, W. K. Maser, N. Tagmatarchis, *ChemSusChem* **2023**, *16*, 202202322.
[115] J. Sun, Z. Zhao, J. Li, Z. Li, X. Meng, *J. Alloys Compd.* **2022**, *918*, 165719.
[116] L. Najafi, S. Bellani, R. Oropesa-Nuñez, M. Prato, B. Martín-García, R. Brescia, F. Bonaccorso, *ACS Nano* **2019**, *13*, 3162.
[117] A. Dymerska, W. Kukułka, K. Wenelska, E. Mijowska, *ACS Omega* **2020**, *5*, 28730.
[118] P. Karfa, R. Madhuri, P. K. Sharma, *J. Mater. Chem. A* **2017**, *5*, 1495.
[119] J. A. Nasir, Z. U. Rehman, S. N. A. Shah, A. Khan, I. S. Butler, C. R. A. Catlow, *J. Mater. Chem. A* **2020**, *8*, 20752.
[120] X. Xu, H. Chu, Z. Zhang, P. Dong, R. Baines, P. M. Ajayan, J. Shen, M. Ye, *ACS Appl. Mater. Interfaces* **2017**, *9*, 32756.

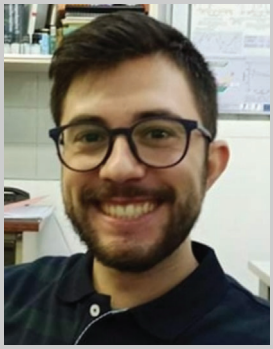

Michail P. Minadakis studied Chemistry at the National and Kapodistrian University of Athens and completed his M.Sc. study in Organic Chemistry in 2019. He is currently a Ph.D. student at the Theoretical and Physical Chemistry Institute of the National Hellenic Research Foundation, in Dr. Tagmatarchis' research group. His main research interest is the study of functionalized carbon nanostructures and transition metal dichalcogenides as electrocatalysts.

Nikos Tagmatarchis is the Director of the Theoretical and Physical Institute, National Hellenic Research Foundation, in Athens, Greece. His research interests focus on the chemistry of 2D nanomaterials and carbon nanostructures, particularly in the context of energy conversion applications. His accomplishments in the area are reflected in a plethora of publications, with multiple citations and numerous invitations to conferences. He has been recipient of the European Young Investigator Award (2004) and Visiting Professor at the Chinese Academy of Sciences (2011-2012), Invited Fellow by the Japan Society for the Promotion of Science (2013-2014 and 2018), and Chemistry Europe Fellow Class 2018/2019.